Report No. TR-91-001-01
December 1991

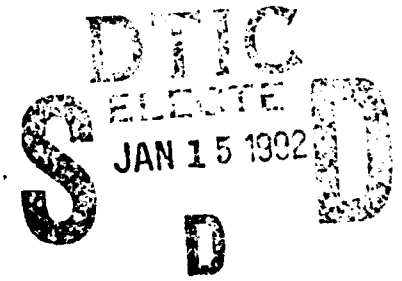

FOCUSED SYNTHETIC MICROWAVE ARRAY FOR MINE DETECTION AND IMAGING

W. J. Graham

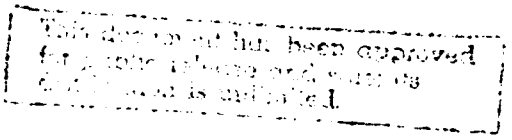

Sponsored by
Belvoir Research Development and Engineering Center
Countermine Technology Division
Contract No. DAAK70-91-C-0040

FINAL REPORT
3 June 1991- 3 December 1991

Graham Research Corp.
2137 Galloway Road
Bensalem, PA 19020

Report No. TR-91-001-01
December 1991

FOCUSED SYNTHETIC MICROWAVE ARRAY FOR MINE DETECTION AND IMAGING

W. J. Graham

Sponsored by
Belvoir Research Development and Engineering Center
Countermine Technology Division
Contract No. DAAK70-91-C-0040

FINAL REPORT
3 June 1991- 3 December 1991

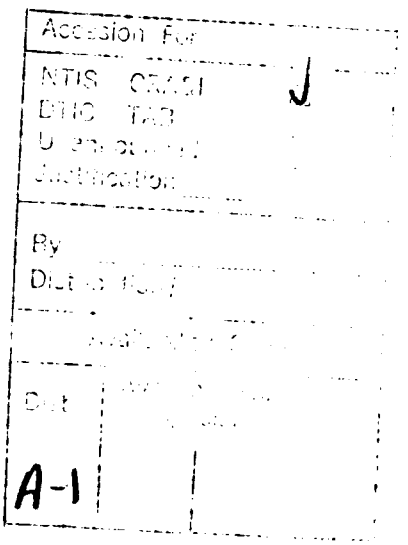

Graham Research Corp.
2137 Galloway Road
Bensalem, PA 19020

UNCLASSIFIED
SECURITY CLASSIFICATION OF THIS PAGE

REPORT DOCUMENTATION PAGE

1a. REPORT SECURITY CLASSIFICATION Unclassified	1b. RESTRICTIVE MARKINGS N/A
2a. SECURITY CLASSIFICATION AUTHORITY N/A	3. DISTRIBUTION / AVAILABILITY OF REPORT
2b. DECLASSIFICATION / DOWNGRADING SCHEDULE N/A	
4. PERFORMING ORGANIZATION REPORT NUMBER(S) TR-91-001-01	5. MONITORING ORGANIZATION REPORT NUMBER(S)
6a. NAME OF PERFORMING ORGANIZATION Graham Research Corp. — 6b. OFFICE SYMBOL (If applicable): N/A	7a. NAME OF MONITORING ORGANIZATION Belvoir Research, Development & Eng. Ctr.
6c. ADDRESS (City, State, and ZIP Code) 2137 Galloway Road Bensalem, PA 19020	7b. ADDRESS (City, State, and ZIP Code) Fort Belvoir, VA 22060-5606
8a. NAME OF FUNDING / SPONSORING ORGANIZATION Belvoir R, D & E Center — 8b. OFFICE SYMBOL (If applicable): N/A	9. PROCUREMENT INSTRUMENT IDENTIFICATION NUMBER Contract No. DAAK70-91-C-0040
8c. ADDRESS (City, State, and ZIP Code) Fort Belvoir, VA 22060-5606	10. SOURCE OF FUNDING NUMBERS PROGRAM ELEMENT NO.: N/A — PROJECT NO.: N/A — TASK NO.: N/A — WORK UNIT ACCESSION NO.: N/A

11. TITLE (Include Security Classification)
FOCUSED SYNTHETIC MICROWAVE ARRAY FOR MINE DETECTION AND IMAGING (U)

12. PERSONAL AUTHOR(S) Graham, William J.

13a. TYPE OF REPORT	13b. TIME COVERED	14. DATE OF REPORT (Year, Month, Day)	15. PAGE COUNT
Final	FROM 6/3/91 TO 12/3/91	1991, December 3	84

16. SUPPLEMENTARY NOTATION
N/A

17. COSATI CODES			18. SUBJECT TERMS (Continue on reverse if necessary and identify by block number)
FIELD	GROUP	SUB-GROUP	FOCUSED ARRAYS, MINE DETECTION, SYNTHETIC ARRAYS

19. ABSTRACT (Continue on reverse if necessary and identify by block number)

This report presents the results of a contract performed by Graham Research Corporation to evaluate the feasibility of a proposed focused synthetic rectangular array for microwave detection and imaging of mines. The proposed technique uses a bistatic antenna system with transmitter and receiver located at the angles of incidence and reflection, respectively of the radiation illuminating the ground. These angles are equal to the Brewster angle of the ground medium so that ground reflections are minimized for vertical polarization. The transmit antenna has a broad beam which illuminates the field of view on the ground. The receiver antenna is a horizontal line array, which forms a rectangular synthetic array by the forward motion of the system. The results of an analytical study are presented, and experimental results are described which give high resolution three-dimensional images of various types of buried anti-tank mines. A system design for a focused rectangular synthetic countermine array is also given. A design of an experimental system for Phase II and a test plan is described.

20. DISTRIBUTION / AVAILABILITY OF ABSTRACT ☐ UNCLASSIFIED/UNLIMITED ☒ SAME AS RPT. ☐ DTIC USERS	21. ABSTRACT SECURITY CLASSIFICATION Unclassified
22a. NAME OF RESPONSIBLE INDIVIDUAL Kelly D. Sherbondy, STRBE-NTD	22b. TELEPHONE (Include Area Code): (703) 664-4992 — 22c. OFFICE SYMBOL: STRBE-NTD

DD FORM 1473, 84 MAR — 83 APR edition may be used until exhausted. All other editions are obsolete.

SECURITY CLASSIFICATION OF THIS PAGE
UNCLASSIFIED

PREFACE

This is the final report on Department of the Army Contract No. DAAK70-91-C-0040 to Graham Research Corporation, sponsored by the Countermine Laboratory of the Belvoir Research, Development and Engineering Center, Fort Belvoir, Virginia. The project was under the direction of Kelly D. Sherbondy of STRBE-NTD. The project manager and principal investigator of this contract was William J. Graham. Additional contributions to the project were made by Donald L. Carlson in the experiment, hardware design and fabrication and the experimental test plan.

Graham Research Corporation wishes to thank Mr. Sherbondy for his interest in this project and for his inquiries regarding the experimental results. The company has welcomed these inquiries, and has enthusiastically responded by supplying initial experimental data to BRDEC with a preliminary analysis of the results.

TABLE OF CONTENTS

LIST OF ILLUSTRATIONS

1.0 INTRODUCTION

1.1 Background

This report presents the results of a contract performed by Graham Research Corporation to evaluate the feasibility of a proposed focused synthetic rectangular array for microwave detection and imaging of mines. The proposed technique uses a bistatic antenna system with transmitter and receiver located at the angles of incidence and reflection, respectively of the radiation illuminating the ground. Furthermore, these angles are chosen equal to the Brewster angle of the ground medium, i. e., the angle at which only radiation having its polarization perpendicular to the plane of incidence is reflected. Consequently, if the antenna polarizations are in the plane of incidence, ideally all of the radiation will be transmitted into the ground and none will be reflected. After reflection from a buried object, the radiation will again be completely transmitted from the ground to air at the Brewster angle.

The transmit antenna has a broad beam which illuminates the field of view on the ground. The receiver antenna is a horizontal line array, perpendicular to the transmit antenna axis. The entire system moves in the direction perpendicular to the horizontal line array, with the array sampling the reflected field at equal intervals in the direction of forward motion, forming a rectangular synthetic array. The array is focused in its near field, and the focal point is scanned in three dimensions below the surface of the ground. A high resolution image is formed which will detect and identify mines and other buried objects.

1.2 Technical Issues

The technical challenge is to develop a mine detection and imaging technique for subsurface land mines using focused array technology that provides the following benefits in a cost effective manner:

1) better than 5 cm resolution in three dimensions

2) subsurface transmission approaching 100%
3) high speed three-dimensional imaging of medium and target
4) ability to detect and identify both metal and plastic mines
5) high rate of forward motion
6) moderate cost

A technique with the potential to provide these benefits is the use of a focused microwave array. Previous obstacles to microwave mine detection have been the large reflection coefficient of the ground, limited depth resolution due to pulse width, the inability to image the mine for identification purposes to reduce false alarms, and the time required for searching a large area. The approach is different from other microwave countermine systems, proposed or realized, in several respects. The first major difference is in the detection system geometry. An obstacle to the use of a monostatic radar system is that the reflections received from the mine target are either vertically scattered or backscattered. In the vertical scattering case the radar system is directly above the mine target, and the target reflections may be largely obscured by the soil surface reflections. Even a short pulse may not distinguish the two if the soil is moist since the mine reflected pulse may be in the sidelobes of the surface reflected pulse. A second difficulty with vertical scattering systems is the height dependence due to the multiple reflections between the radar and the soil that causes standing waves. Another difficulty is the short standoff distance due to vertical detection. These problems are sometimes avoided by using a monostatic backscatter system in which the radar receives the backscattered reflections from the mine at an oblique angle. Here, however, another difficulty is apparent if one examines the backscattering characteristics of anti-tank mines. The beamwidth of the scattering pattern is generally limited to 10 degrees from the vertical so that the backscattering to a radar at any greater angular deviation from vertical incidence will be too low.

These difficulties have been largely overcome by work of the principal investigator of this program. A method of mine detection is proposed that uses a bistatic oblique forward scattering geometry with a focused rectangular synthetic array used as a receiver. The frequency and dimensions are chosen

for high resolution, while forward scattering at the Brewster angle will reduce ground reflections to zero. High depth resolution is obtained from the depth of field (axial beamwidth) of the array focus. Resolution can be increased and near-field sidelobe level can be reduced in range and angle using techniques developed by the principal investigator. Three-dimensional imaging is done by digital focusing and beamforming with the array at high speed.

1.3 Proposed Solution

The proposed countermine technique is based upon focused array technology developed by the principal investigator [1], [6], [5], [7], and upon the previous focused countermine array theoretical and experimental work. The technology uses proven techniques of near-field imaging and focused array pattern analysis and synthesis to form multiple simultaneous focused beams with high resolution in three dimensions. This technology is combined with the use of oblique forward scattering at the Brewster angle in order to reduce surface reflections.

The system technique proposed is illustrated in Fig. 1. The coordinate system shown has its origin on the ground directly below the transmitter. Depth is represented by the z coordinate which increases with depth, while x increases toward the horizontal line array receiver and the y axis is parallel to the line array. A bistatic radar system is depicted which consists of a wide beam horn antenna transmitter at height h above the ground, for illumination of a large surface area, and a focused horizontal line array receiver at height h . Both are directed obliquely to a common area on the ground (x-y plane) below and between them. The oblique angle is chosen to be near the Brewster angle for the medium [2], i. e., the angle at which a wave polarized in the plane of incidence is completely transmitted into the medium, as illustrated in Fig. 4. For this reason, the polarization chosen for the system is in the plane of incidence, i. e., the x-z plane. Although the beamwidth of the array elements covers a range of angles about the Brewster angle, the proximity to the Brewster angle still results in a large reduction in surface reflections.

The entire radar system is mounted on a vehicle and moves in the x

FOCUSED COUNTERMINE ARRAY CONFIGURATION

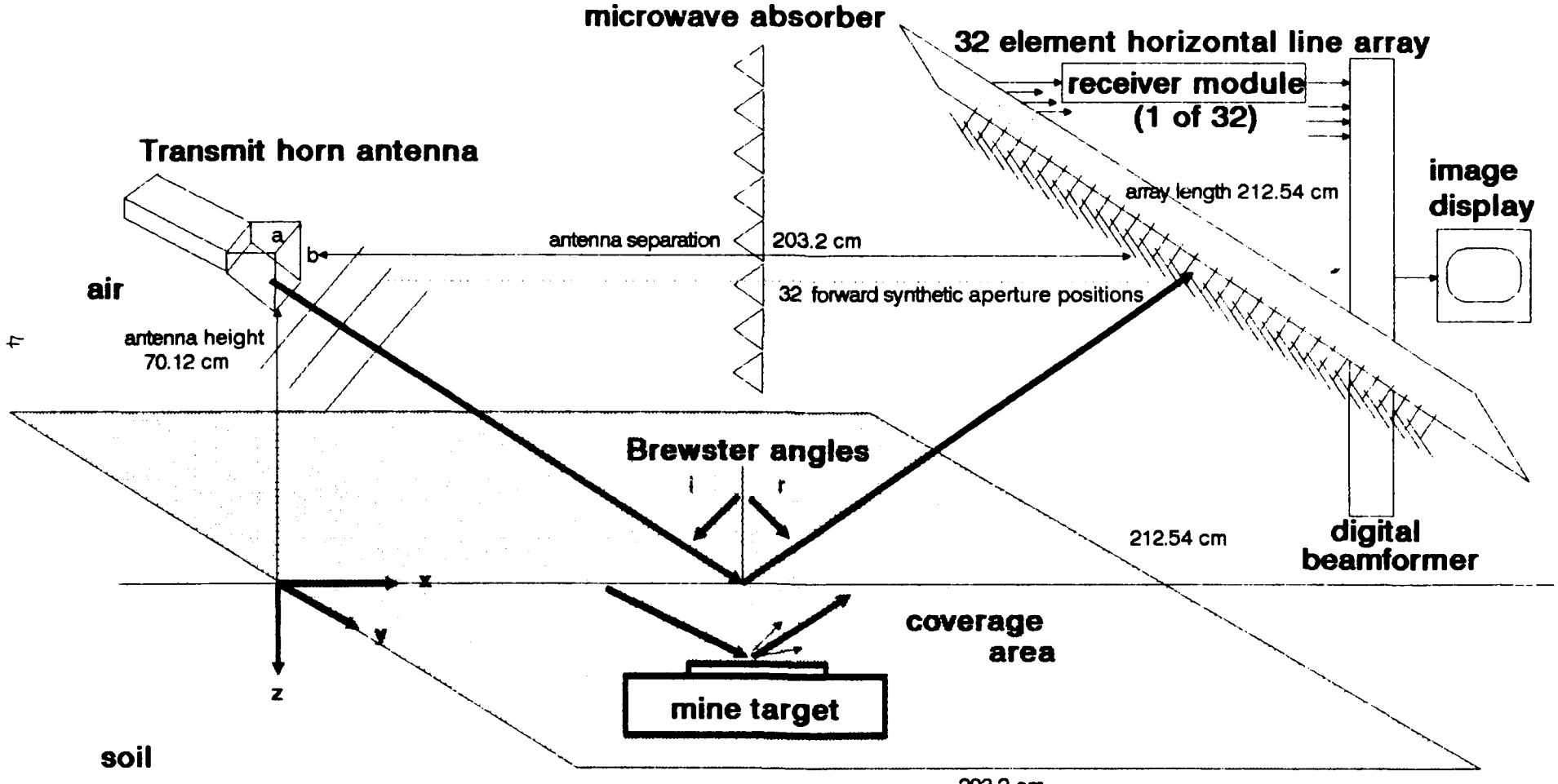

Fig. 1. Geometry and components of focused countermine array system.

tal line array elements sample the reflected field at equally spaced points forming a synthetic aperture in the x direction, as shown in Fig. 2. This procedure in effect forms a horizontal rectangular receiver array. This rectangular array is then focused by phase shift correction for the phase curvature of the wavefront from the focal point to the array. The array then forms a high resolution image by scanning the focused beam over the illumination area of interest, and the process continues by adding new synthetic elements as the system continues to move in a forward direction, as illustrated in Fig. 3. A system diagram of this process is given in Fig. 33.

A focused array has a three-dimensional beam with dimensions in the horizontal plane and in depth. The vertical dimension of the focused beam is called the depth of field, and allows the array to resolve objects in depth. The horizontal beamwidth and depth of field are inversely proportional to the array size in wavelengths, and decrease as the range to the focal point decreases. Thus, a focused array can achieve a very high resolution in its near field by forming three-dimensional resolution cells as seen in Fig. 3.

After the horizontal line array elements receive the reflected radiation from the medium, the scanning process is accomplished when the element data is digitized and sent to a central processor. Here three-dimensional focused digital beamforming is done using Fresnel transform approximations developed in [1]. These approximations allow the separation of radial and angular coordinates so that Fourier transform methods can be used to focus the array and compute the near-field focused array response. Near-field pattern synthesis methods developed by the principal investigator [5], [7] are used to increase focal resolution and reduce sidelobe level in both range and angle.

1.4 Advantages

The technique of a focused array countermine system has the potential to provide the benefits listed in section 1.2. First, the ability to achieve high resolution in three dimensions using high speed three-dimensional imaging is the key feature of the proposed technique. A resolution limit of one-third wavelength can be obtained with a focused array. Resolution in depth is obtained through the depth of field of the focused array beam rather than

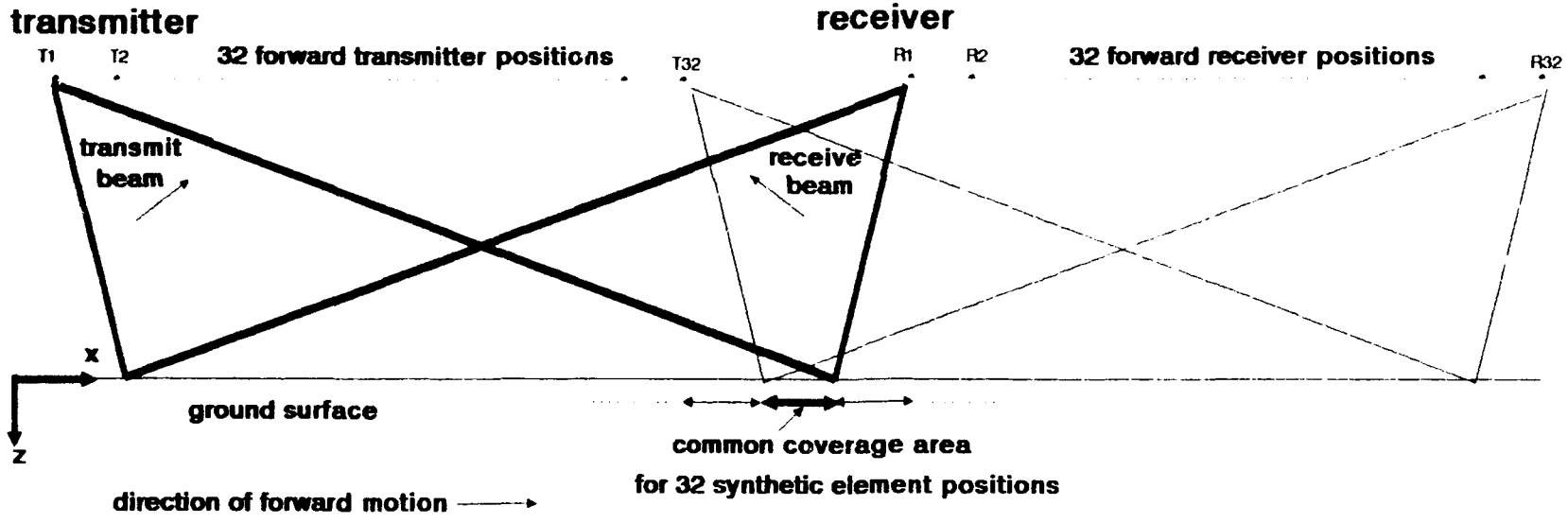

Fig. 2. Formation of synthetic array by forward motion of system (side view).

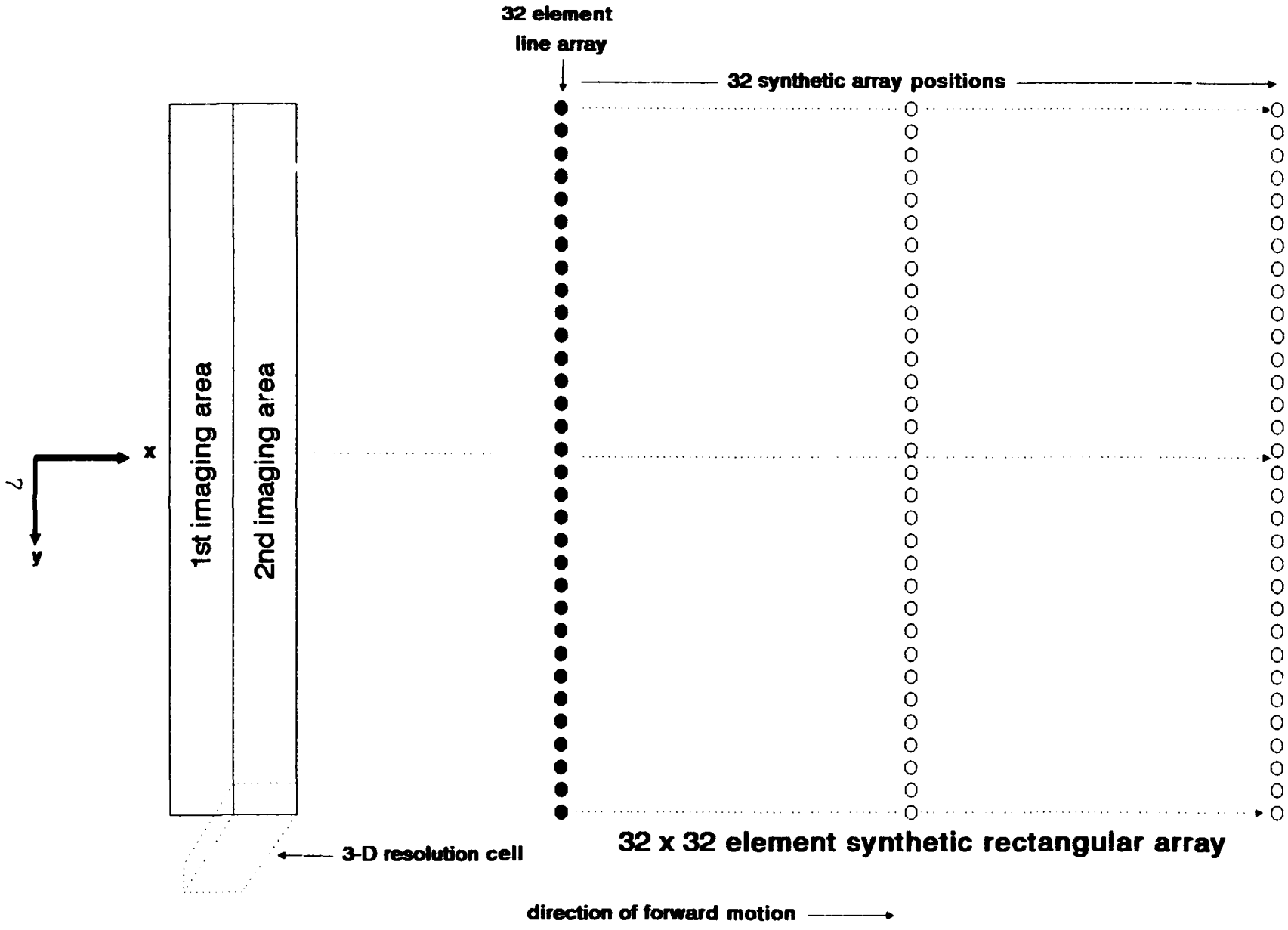

Fig. 3. Synthetic rectangular array and imaging area (top view).

FOCUSED ARRAY GPR IMAGING

PROPAGATION GEOMETRY

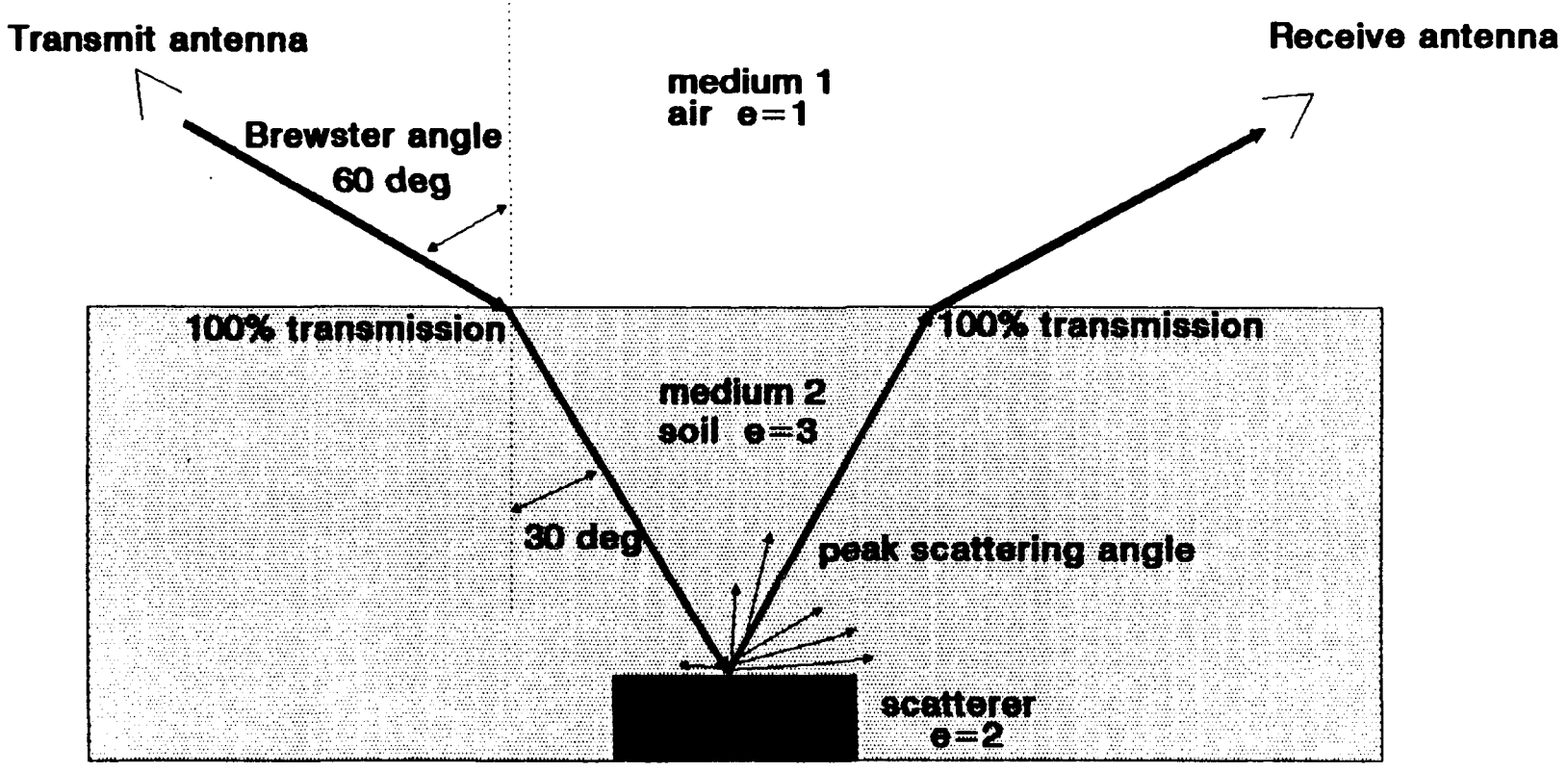

Fig. 4. Brewster angle propagation geometry.

resolution of 5 cm at S-band frequencies. Resolution in the longitudinal direction (direction of forward motion) is obtained from the synthetic aperture formed by the motion of the horizontal receive array, effectively making it a rectangular array.

The imaging process requires that the receiver array elements phase shift and sum the ground reflected signals so that the array forms a focused beam at the desired image point, i. e., the array has a maximum sensitivity at that point. This beam is scanned to a number of horizontal image points by applying the proper phase shifts to the element signals. This beamforming process can be computationally intensive. However, the results of [1] and [7] allow near-field digital beamforming at each range by forming simultaneous focused horizontal beams using the Fresnel transform approximation computed by a spatial fast Fourier transform (FFT). The beamforming is done using the baseband in-phase and quadrature signal components. An advantage of this technique is the ability to maintain a high rate of forward motion because of the reduction in computations using the FFT. Since the imaging is done at high speed using digital beamforming, the limitation on forward speed will be the time required to stop the vehicle in the forward distance to the detected mine. For this reason, the detection should be made at as large a distance as possible consistent with the geometrical requirements of a focused array and with the mechanical requirements for mounting it.

The use of bistatic oblique forward scattering is a unique technique with the advantage of reducing surface reflections. This is accomplished by using a polarization in the plane of incidence (x-z plane) at the Brewster angle [2], as shown in Fig. 2. The surface reflections will decrease greatly depending on the dielectric constant and conductivity of the soil. The oblique forward scattering from a mine, however, has been shown experimentally in our previous work to remain near its peak level out to the Brewster angle [8].

1.5 Technical Objectives

The objective of the proposed work was to evaluate the feasibility of a bistatic oblique forward scattering radar system using a rectangular focused synthetic array. Our previous work considered only a one-dimensional horizontal line array and obtained only one-dimensional surface images of the mine. By using the forward motion of the detection system, the horizontal line array can synthetically form a horizontal rectangular array for high-resolution two-dimensional imaging. An obvious advantage of this approach is the very low cost of the system, since the horizontal line array will use digital beamforming rather than hardware beamforming, and the rectangular array is formed only through the motion of the line array.

The effort was to analytically determine the feasibility and performance of the technique of using a rectangular focused synthetic array for high resolution three-dimensional mine imaging. Since a complete mine detection facility already existed, and hardware was in place for horizontal line array measurements, the Phase I effort included experiments for verification of the synthetic aperture technique.

An additional objective of the proposed work was the development of a conceptual radar system design for evaluation of system feasibility. This included such considerations as transmitter type, design, and performance required, ground coverage, receive array hardware and software, signal processing, and speed of forward motion. This will provide the basis for a second level system design in Phase II.

A final objective of the work was the design of an experimental test system for Phase II verification of Phase I results, and the development of a test plan.

The specific objectives were:

1) to analyze and apply synthetic aperture techniques to form a focused rectangular array using the forward motion of a horizontal line array

2) to experimentally verify some of the aspects of the technique

3) to analyze the forward scattering characteristics of buried anti-tank

mines and soil based upon experimental data

4) to develop a conceptual radar system design for a rectangular focused synthetic array countermine system to prove feasibility

5) based upon the results of 1) to 4), design an experimental test system that will be fabricated and tested during Phase II.

The questions that were answered in meeting these objectives are

1) can two-dimensional surface images be obtained that allow determination of shape information for identification and classification of both metal and plastic anti-tank mines? Experimental high resolution surface images were obtained of buried mines that showed distinctive characteristics in the scattering patterns that allowed positive identification and classification.

2) what is the resolution attainable by the system? The experimental results verified the theoretical predictions in giving about 5 cm resolution in the images of buried objects.

3) what is the maximum speed of forward motion that can be sustained with reliable detection of mines? The results of the system design study indicate no limit on speed due to the data collection, processing, and imaging time required.

4) what is the cost of the system? Because of its simplicity of design, the system will be very low cost. Therefore the Phase II program will design, fabricate, and test a prototype of the proposed system.

1.5.1 System Design

The first technical objective was to evaluate analytically the proposed synthetic focused array technique. The proposed technique differs from our previous work by the formation of a synthetic rectangular receive array. The basis of the analysis was the previous work using a horizontal line array receiver. The proposed work extended this by allowing the horizontal line array to move in the forward direction with each of its array elements sampling the field at equal intervals. The size of the array that can be synthetically formed depends upon the ground area to be imaged with that array. As

shown in Fig. 2, this is dependent upon the coverage area of the transmit antenna. As the system and this antenna moves in a forward direction, its coverage area also moves forward, so that the addition of synthetic array elements causes a decrease in common coverage area of the synthetic array. A small common coverage area can be chosen, such that a larger synthetic array can be used giving a higher resolution in the longitudinal direction. An example would be a coverage area whose longitudinal dimension is equal to the longitudinal synthetic array element spacing, as illustrated. Thus, as the system moves forward by this distance, a new imaging area is defined, and a new synthetic array is formed by adding a new first element, and dropping the last. This allows a larger synthetic array with no redundancy in the imaging area.

A part of this objective was a study of the near-field pattern characteristics of the rectangular focused array. This included a consideration of the effects of refraction on the pattern. The different dielectric constant causes the ray paths from the array elements to the focal point to refract, which changes the total phase from the geometric direct path phase. This may result in some defocusing of the beam, although our previous experiments have shown that the effect is negligible with the horizontal array. If the effect is too large with the rectangular array, then some correction may be necessary in order to improve the beam focus and the image.

The focusing characteristics of the rectangular array were also analyzed. These characteristics are defined in Section 2.2. The depth of field, which is the beamwidth in the depth coordinate, and horizontal resolution were determined for a given array size by computation of a contour plot shown in Fig. 7 and described in Section 2.2. The effect of scanning the array focus in the horizontal plane and in depth was determined by computation of the response of the array to a point source reflector as the array is scanned throughout a volume. The sidelobes of a focused array exist in three-dimensions, i. e., in both angle and depth. William J. Graham has done considerable research in the focal region characteristics of focused arrays, including a method for reducing these sidelobe levels, and for synthesizing the focused array pattern in depth in the same manner as conventional techniques used for far-field synthesis in angle. This permits the reduction of the high axial

sidelobes often seen in focused array patterns.

In parallel with this analytical effort, experiments were performed during Phase I to test some of the aspects of the synthetic aperture technique. The existing mine detection test setup was used to synthetically move a single antenna element to form a synthetic line array in both the x and y directions as illustrated in Fig. 18. Experiments were performed with buried metal and plastic anti-tank mines using a stationary transmitter and moving a single wide beam antenna element in the forward direction, sampling the field at several equally spaced points, and forming a synthetic horizontal line array in this direction. A synthetic line array was also formed in the perpendicular direction with the target and medium undisturbed. This permitted the outputs of the orthogonal arrays to be combined. The sampled data was then input to the beamforming and imaging program to form images of the mine in three mutually orthogonal planes, for each of the line arrays, and for their combination. The orthogonal planes are the horizontal x-y plane, the vertical x-z plane, and the vertical y-z plane, defined by the coordinate system shown in Fig. 1. Some modification of the beamforming software was required to accommodate the difference in geometry of the x-collinear horizontal line array. This data allowed a useful evaluation of some of the problems which may be encountered in the synthetic array system. It also demonstrated the characteristics of the buried mine images in the x direction and in a horizontal surface plane, and any anomalies that may appear.

Another objective of the work was the analysis of the existing oblique forward scattering data of buried anti-tank mines. Much data has been taken by Graham Research using the experimental mine detection facility at the University of Pennsylvania Valley Forge Research Center. The data consists of reflections from soil and from buried M15 metal and M19 plastic mines at L-band and S-band frequencies using a forward scattering geometry at the Brewster angle. This data was measured by a horizontal line array in the y direction, giving soil and mine images in the y dimension as a function of depth. There are questions to be answered about these reflection characteristics and how they affect the design of the proposed synthetic focused rectangular array. These questions concern the effect of refraction on the mine images and the additional information provided by images in the other two

orthogonal planes. This data was analyzed to help determine the feasibility of the proposed countermine system.

The next technical objective was the development of a conceptual radar system design for the focused rectangular synthetic countermine array. The purpose was to prove feasibility of the technique by showing that the proposed system can be designed to achieve the desired performance with state of the art components at a reasonable cost. The system geometry depends upon the results of the previous tasks. This determines the feasible separation of transmit and receive arrays, the angle of incidence, and the required distance of the arrays from the surface. The factors that influence these parameters are the optimum forward scattering angles for various mine types and soils, the desired resolution, and the power density required at the target for detection. The resolution goal is on the order of centimeters in range, depth and cross-range. This allows many resolution cells to be formed on a mine for imaging and identification and also for reduction of clutter from ground reflections. The entire search area need not be imaged with this resolution for detection purposes. Lower resolution can be used for detection, and scanning can be switched to a high resolution mode for actual imaging of the mine. This procedure will save data processing time.

Array beamforming and processing considerations were the major task in the system design effort. Synthetic array systems require a consideration of the interrelationships of system geometry, speed of forward motion, resolution, image area, etc. The array beamforming requires an analysis of rectangular focused array pattern characteristics, and an evaluation of the application of near-field digital beamforming techniques developed by the principal investigator. Focused array pattern synthesis techniques developed by the principal investigator can be used for the improvement of resolution and the reduction of sidelobe level.

The system design also considered system frequency. Our previous work has considered L-band and S-band. L-band frequencies have been ruled out for mine imaging purposes because of the long wavelength and resultant poor resolution. S-band (3.5 GHz) results have been very good, showing the ability to both detect and image metal and plastic mines. The wavelength in dry sand was 5.4 cm and gave several resolution cells on the

surface of the mines. An upper limit on frequency for mine detection is probably C-band (4-6 GHz) since attenuation and phase error problems are probably too large beyond this range. S-band has been selected for the system design and Phase II experiment.

Finally, the system design effort considered methods of mounting the array system on a search vehicle. This is important since searching is desired in a forward direction and the transmitter and receiver arrays must be mounted ahead of the vehicle. Since the system will be very light in weight, it can be mounted on lightweight arms extended from a vehicle.

1.5.2 Experimental Design

Design of a Phase II test system for mine detection was the final objective of the proposed work. In Phase II this test system design will be fabricated and used for an experimental verification of the proposed technique. The Phase II experiments will be done at the mine detection facility at the Valley Forge Research Center (VFRC) of the University of Pennsylvania under the direction of the principal investigator. This center has the facilities, equipment and personnel required for the conduct of radar and antenna measurements at various microwave frequencies.

The purpose of the test system is to verify some of the most important detection system techniques. These include synthetic aperture, array focusing and pattern synthesis, digital beamforming, high resolution imaging, and forward scattering detection. The test system will include a transmitter and a horizontal line array receiver. The entire system will be movable in order to test the formation of a rectangular synthetic array. A low power transmitter in the desired frequency range would be used for illumination of the target and medium. The receiver horizontal line array would have its antenna elements switched to a digitizer for sampling and storage of element waveforms.

The purpose of the experiment would be to test the synthetic aperture concept using hardware that closely resembles the proposed system design. Since transmitter and receiver equipment is available in several frequency ranges, the design will use existing transmitter and receiver equipment wherever possible. Available equipment includes narrow pulse transmitters,

receivers, and antenna and microwave hardware at L, S, X, and Ku bands. The experiment will be performed in the outdoor subsurface mine detection facility where the Phase I experiments were performed. This at present consists of L-band and S-band transmitters and antennas, with an HP 54120T 20 GHz sampling oscilloscope for digitizing array element data, with an interface with an HP 9816 computer where it is transferred to an 80386 20 MHz computer with math coprocessor for analysis, signal processing, and three-dimensional image generation on the high resolution VGA graphics system.

For related antenna and array pattern measurements, an azimuth positioner and Scientific Atlantic chart recorder is available for the measurement of antenna and RCS patterns. Narrow pulse RCS measurement of mines also could use the existing HP 54120T 20 GHz sampling oscilloscope interfaced with the HP 9816 computer for digital recording and RCS pattern display.

1.6 Summary of Results

The Phase I program, especially the synthetic array experiments, have produced results which far exceeded expectations. The analysis has shown that a focused rectangular synthetic array can be designed with a minimum of hardware components of relatively low cost while maintaining the highest detection capability and resolution in any known countermine system. These results have been verified in the synthetic aperture experiments in which images of the top surface of plastic and metal mines have demonstrated resolution of 5 cm and detectability of anti-tank mines with a signal-to-clutter ratio of 12.5 dB for the plastic mine and 23.3 dB for the metal mine. Analysis of existing mine scattering data has indicated that for oblique angles of incidence near the Brewster angle, there is a significant increase in mine detectability and signal-to-clutter ratio over conventional vertical incidence.

A conceptual focused synthetic array system design shown in Fig. 1 has been developed which incorporates these results. The system covers a field of view of about 2 meters square at each position. The antenna systems are simple, requiring a small horn antenna as the transmitter, and 32 vertical half-wave dipoles in the receiver array. The receive array utilizes digital beamforming so that no phase shifters or power combiners are required. Each

element has a simple receiver module with an A/D converter shown in Fig. 34, followed by a high speed processor which forms multiple simultaneous beams in the horizontal as the sytem progresses in the forward direction. The forward motion forms a 32 element synthetic array in this direction as illustrated in Fig. 2 making an equivalent 32 x 32 element rectangular focused array. This 1024 element array is focused and scanned in 5 cm increments in both x and y for the chosen depths as shown in Fig. 3. The beamforming has been simplified so that only 32 new horizontal beam computations need be performed at each new forward beam position in 5 cm increments. This drastically reduces the computation load so that there is essentially no limitation on the speed of forward motion because of processing time.

Because of the simplicity of the proposed system design, it was decided to design, fabricate and test during Phase II, an experimental system which matched the design parameters of the proposed system as closely as possible. The Phase II experimental program will use the proposed system transmitter horn antenna design and the 32 element half-wave dipole receiver array, in the same geometry as the proposed system. The system will be movable in the forward direction guided by a track, with the system sampling the field in the forward direction to form a synthetic rectangular array of the same size as the proposed system. The main difference between the Phase II experiment and the proposed system design will be the use of a single receiver module shared by all 32 array elements as shown in Fig. 35. The array elements will be electronically switched to the single receiver module in sequence, with the output of the module stored in a data aquisition processor until all elements have been sampled. The line array then moves to the next sampling position, where the procedure is repeated, until the entire 1024 element rectangular array is synthetically formed. Imaging is performed in accordance with the procedure described previously, for each sequential forward position in 5 cm intervals.

2.0 ANALYTICAL STUDY

The purpose of the analytical study was to determine some of the basic feasibility issues of the proposed focused rectangular synthetic array. Some

of these issues are resolution, effect of refraction and conductivity, and the data processing load.

An objective of the proposed system is to obtain a high enough resolution by the use of a focused array, that a mine could actually be identified by the characteristic signature of its image. A unique scattering pattern would be associated with all types of mines and other buried objects, so that not only could they be detected, but they could be specifically identified, and the false alarm rate would be very small.

The effects of refraction and conductivity on the system performance are important factors since they may affect the resolution and localization of a mine. These effects have been analyzed by comparing actual mine images with the refraction included in the array focusing and imaging. The effect of conductivity on soil reflections was also determined by analyzing measured soil reflections as a function of incidence angle for moist soil.

The data processing load is a major factor in determining the allowable speed of forward motion. This has been analyzed in section 5.4. A mathematical simplification called the Fresnel transform approximation is described below, and may provide a further reduction in the computation load.

The theoretical development of the focused array pattern, the Fresnel transform, and the characteristics of focused arrays are presented in the following sections to analyze the above issues.

2.1 Radiated Field in the Fresnel Region

The exact expression for the radiated electric and magnetic fields at any point R in an unbounded region, due to a current distribution within a volume V, are given by Stratton [2] as

$$E(x,y,z) = (1/4\pi)\int_V [(\rho/\epsilon_0)\nabla G - j\omega G\mu_0 J]\, dV \qquad (1)$$

$$B(x,y,z) = (1/4\pi)\int_V \mu_0 J \times \nabla G\, dV \qquad (2)$$

$$G = e^{-jkR}/R.$$

Using the continuity equation, (1) can be written in another version as

$$E(x,y,z) = (1/4\pi)\int_V (1/j\omega\epsilon_0)[(J \cdot \nabla)\nabla G + k^2 GJ]\, dV \qquad (3)$$

This can be expanded in terms of a unit vector R from the source to field point using the identity

$$(J \cdot \nabla)\nabla G =$$
$$\{(J \cdot \hat{R})\hat{R}[(3/R)(jk + 1/R) - k^2] - (J/R)(jk + 1/R)\}e^{-jkR}/R. \qquad (4)$$

For values of kR >> 1, terms of order higher than 1/R can be neglected, and E becomes

$$E(x,y,z) = (-j\omega\mu_0/4\pi)\int_V [J - (J \cdot \hat{R})\hat{R}]e^{-jkR}/R\, dV. \qquad (5)$$

Note that this restriction on R indicates that (5) is generally valid only for near-field distances in the Fresnel region, and is *not* valid for arbitrarily small distances in the near field. The error in neglecting higher order terms is on the order of 1/kR.

For an array of radiating elements which are identical in both geometry and orientation, the current distribution on the i^{th} element, J_i, can be expressed in terms of a normalized current distribution in the individual element coordinate system, J_0, and the total current at the terminals of the element, I_i, as

$$J_i = (I_i/I_0)J_0. \qquad (6)$$

The electric field now becomes

$$E(x,y,z) = (-j\omega\mu_0/4\pi)\sum_{i=0}^{N}(I_i/I_0)\int_{V_i}[J_0 - (J_0 \cdot \hat{R}_i)\hat{R}_i]\exp(-jkR_i)/R_i\, dV_i. \qquad (7)$$

In terms of the distances r and R_{0i} from the element origin to the source point and field point, respectively,

$$R_i = R_{oi} - r \cdot \hat{R}_{oi} \tag{8}$$

since R_i is in the element far field. The value of E then becomes

$$E(\rho,\theta,\phi) = \sum_{i=0}^{N} (I_i/I_0)\exp(-jkR_{oi})/R_{oi}\ E_i(\theta,\phi) \tag{9}$$

where the element pattern is

$$E_i(\theta,\phi) = (-j\omega\mu_0/4\pi)\int_{V_i} [J_0 - (J_0 \cdot \hat{R}_{oi})\hat{R}_{oi}]\exp(-jkr \cdot \hat{R}_{oi})\ dV_i. \tag{10}$$

Expression (9) is the total electric field at a point (ρ,θ,ϕ) in the Fresnel region from the array origin reference. The element pattern contribution given by (10) is different for each element and must be retained within the summation in (9).

If the element currents are adjusted in phase to focus the array at a focal length R_f in the Fresnel region, the measured field expression (9) becomes

$$E(\rho,\theta,\phi) = \sum_{i=0}^{N} (I_i/I_0)\exp[-jk(R_{oi}-R_{fi})]/R_{oi}\ E_i(\theta,\phi) \tag{11}$$

In order to show the relationship to the Fourier transform, the Fresnel transform [1] will be introduced. Consider the Fresnel region field due to a continuous line source [2]

$$E_\theta(\rho,\theta) = (-j\omega\mu_0/4\pi)\int_{-L/2}^{L/2} I(x)\cos\theta' e^{-jkR}/R. \tag{12}$$

If this line source could be focused in the Fresnel region at $(\rho_0,0)$, then the field at ρ_0 is

$$E_\theta(\rho_0,\theta) = (-j\omega\mu_0/4\pi\rho_0)\cos\theta\int_{-L/2}^{L/2} I(x)\exp[-jk(x^2\sin^2\theta/2\rho_0 - x\sin\theta)]\ dx. \tag{13}$$

This approximation is generally known as the Fresnel approximation, where radial distances have been expanded and terms higher than second order have been neglected. It is well known that for small values of θ, i. e., generally less than 10 degrees, this expression approximates the far-field pattern, and is called the small-angle approximation. However, from Erdelyi's theorem [3] and from the work of Taylor in asymptotic forms of line source patterns [4], it has been shown in [1] that for all values of θ, the integral in (13) can be expressed as

$$E_\theta(\rho,\theta) = (-j\omega\mu_0/4\pi\rho_0)\cos\theta \exp[-jk(L/2)^2\sin^2\theta/2\rho_0]\int_{-L/2}^{L/2} I(x)e^{-jkx\sin\theta}dx. \quad (14)$$

Expression (14) is known as the Fresnel transform of the current distribution, and is valid for

$$\begin{aligned} &\rho_0 > L(L/2\lambda)^{1/3}, \text{ for } L>16\lambda, \text{ or} \\ &\rho_0 > 2L, \qquad\qquad \text{for } L<16\lambda. \end{aligned} \quad (15)$$

For smaller angular ranges like those used in the proposed system, the range of validity extends much closer to the array. The significance of (14) is that it is proportional to a Fourier transform. Thus the entire near-field pattern in both amplitude and phase can be determined from a Fourier transform of the current distribution. Analogously, the response of the focused array to reflections from near-field targets is also a Fresnel transform, and can be computed using near-field digital beamforming with simultaneous focused beams computed by a spatial fast Fourier transform in the Fresnel region.

2.2 Characteristics of Focused Arrays in the Fresnel Region

Focusing an aperture has its origin in optics, where a lens focuses parallel light rays at its focal point. This focal point has a lateral resolution and axial resolution (depth of field) determined by the size of the lens and the wavelength of light. An analogy in antenna theory is a focused array. In this case, the rays arriving at the array from a fixed point in the near field are shifted in phase by the array and combined in phase. The fixed point

becomes the focal point of the array, having the optical field characteristics of lateral resolution and depth of field. Thus, a source located at this point will be focused by the array and combined in phase by the array elements, while sources outside the focal point will be received at a reduced level determined by the sidelobe characteristics of the array.

The importance of a focused array is in its resolution characteristics, and in its three-dimensional field pattern characteristics. The angular beamwidth of the array is approximately equal to the ratio of wavelength to array size, while the axial beamwidth (depth of field) is approximately proportional to the square of this ratio, and is given as [5]

$$\Delta\rho = 7\lambda f^2/[L^2-(3.5\lambda f/L)^2] \tag{16}$$

The hyperfocal distance, f_h, i. e., the value of f where the array is in focus out to infinity is determined by setting $\Delta\rho = \infty$ in (16) which gives

$$f_h = L^2/(3.5\lambda). \tag{17}$$

Since the pattern is three-dimensional, the sidelobes also exist in both angle and range, those in the axial coordinate in front of and behind the focal point being called frontlobes and backlobes, respectively. It is an important characteristic of an array focused in the Fresnel region at distances which satisfy (15), that at the focal radius the angular pattern of the focused array is the same as its far-field pattern as shown by the development of Section 2.1. Another characteristic of a focused array is known as the focal point shift. The focal point is truly the point for which the array elements are in phase, and the pattern at this focal radius is proportional to the far-field pattern according to theory. However the focal point does not correspond to the amplitude maximum of the pattern. The maximum actually occurs at a distance closer than the focal point because of the additional affect of spherical spreading of the wavefront. This phenomenon is sometimes referred to as a focal point shift. The conclusion is that the maximum amplitude of a focused array pattern does not occur at its true focal point, and that this focal point cannot be found empirically by calibration or maximization of the source signal.

Fig. 7 shows a contour plot of the focal region of a 22 element linear

array, focused in the Fresnel region at a distance of 15 wavelengths. The gray levels represent amplitude in 3 dB increments, with the maximum at the focused beam shown as black, while amplitudes below -45 dB are white. The ordinate is the sine space variable, u, whose range represents the complete angular semicircle in front of the array.

In this graph, the depth of field and angular beamwidth is evident, as is the region of the sidelobes. Sidelobes can be seen to appear in both dimensions of the pattern. A line drawn through the focal distance of 15 wavelengths will represent the focal radius, and the values of the focused contour pattern on that line will correspond to the image distance.

2.3 Three-dimensional Near-field Focused Patterns

Fig. 7 has demonstrated a contour plot of the focused near-field pattern of the 22 element horizontal line array parallel to the y axis as a function of u and range. A three-dimensional visualization of the spatial response of a focused array requires computation of the response to a point source, i. e., the point spread function, in the three orthogonal planes. These are presented in Fig. 23 for the horizontal line array parallel to the x axis shown in the Phase I experimental configuration of Fig. 18. The corresponding patterns for the horizontal line array in the y direction as shown in Fig. 18, are given in Fig. 24. The composite crossed line array configuration response is given in Fig. 22. This gives the best representation of the resolution possible with the rectangular array, excepting the previously described horizontal beam spreading caused by the x-array, which would disappear with the filled rectangular array. The indicated resolution in both the x and y dimensions is about 5 cm.

2.4 Effects of Refraction and Conductivity

Figs. 11 and 12 show images of subsurface mines which will be described in Section 3.3. Figs. 16 and 17 illustrate the difference in the mine images when refraction is included in the computations. The effect is to increase the image resolution in depth, giving a much better indication of the target extent in that dimension. The conclusion is that correction for medium

refraction should be included in the beamforming computations to optimize the resolution.

The effect of a conductive medium, such as would exist with any moisture content in the soil would be to make the medium dispersive. This would be especially important in the microwave region where soil exhibits a more dispersive nature. This dispersion would totally rule out the use of a narrow pulse system because of the resulting pulse distortion. The proposed system would use a continuous waveform so there would be no effect of dispersion.

3.0 SCATTERING DATA ANALYSIS

3.1 Anti-Tank Mine Radar Cross Section

The importance of RCS measurements of anti-tank mines in both a forward scattering and backscattering mode is to determine the reflections that can be expected for a given transmitter and receiver configuration. In order to determine the feasibility of the proposed bistatic oblique propagation geometry, data was analyzed that consisted of previously measured forward and backscattering radar cross section of anti-tank mines. Conclusions from this analysis are that there is a wide angle of forward oblique scattering beamwidth for the mines tested, while the backscattering beamwidth is very small. This indicates that a forward oblique scattering system using Brewster angle propagation will generally have a much higher level of mine reflectivity than oblique backscattering.

3.2 Soil Reflection Characteristics

The Brewster angle propagation geometry is illustrated in Fig. 4. Ideally if radiation polarized in the plane of incidence is incident on a dielectric plane interface, there will be complete transmission into the dielectric at the 90 degree complement of the Brewster angle. Upon reflection at this angle from a subsurface plane interface, the wave will be completely re-transmitted into free space at the Brewster angle to the receiver.

Fig. 6 shows the reflected field amplitude as a function of angle of

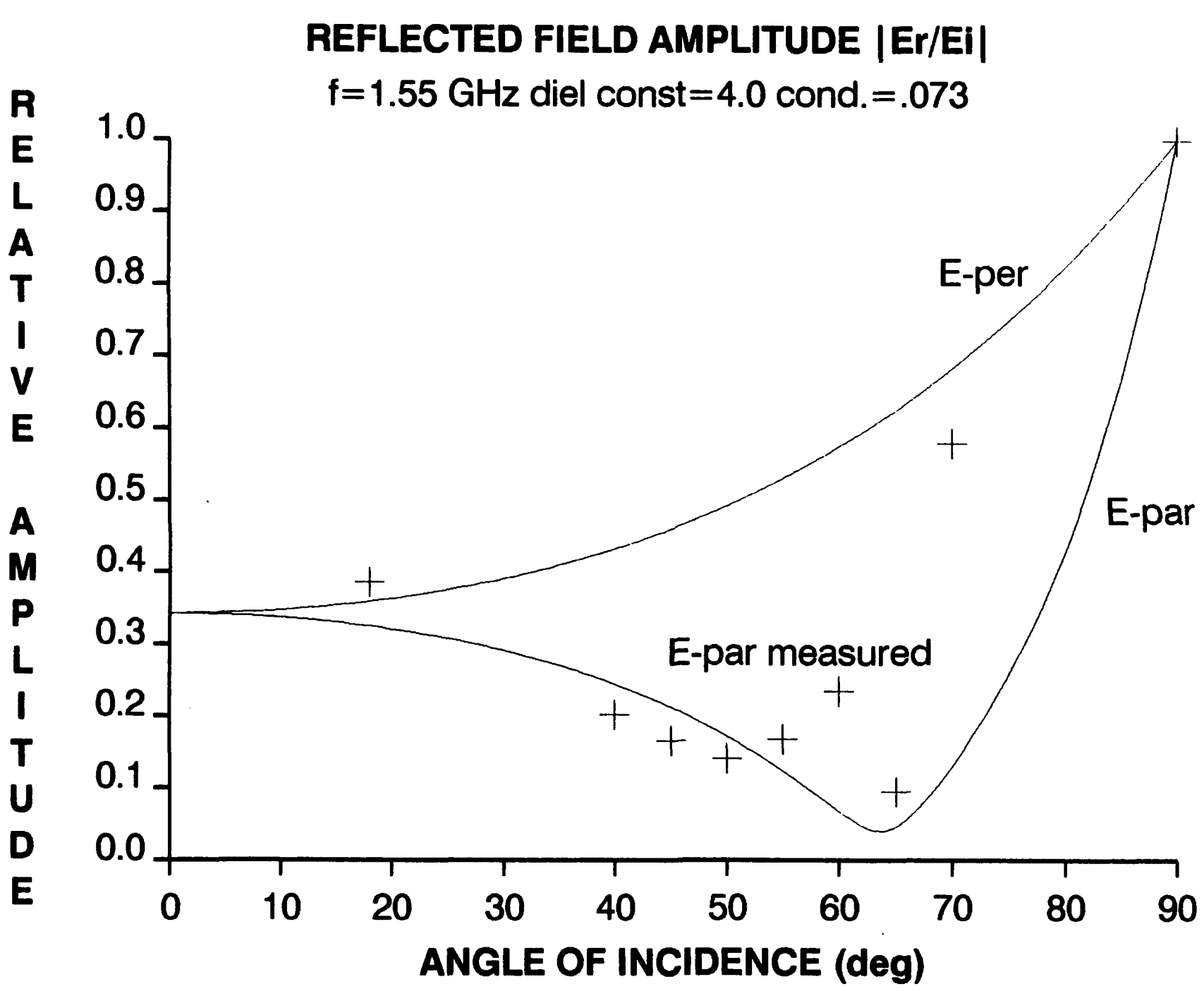

Fig. 5. Reflected field amplitude, f=1.55 GHz.

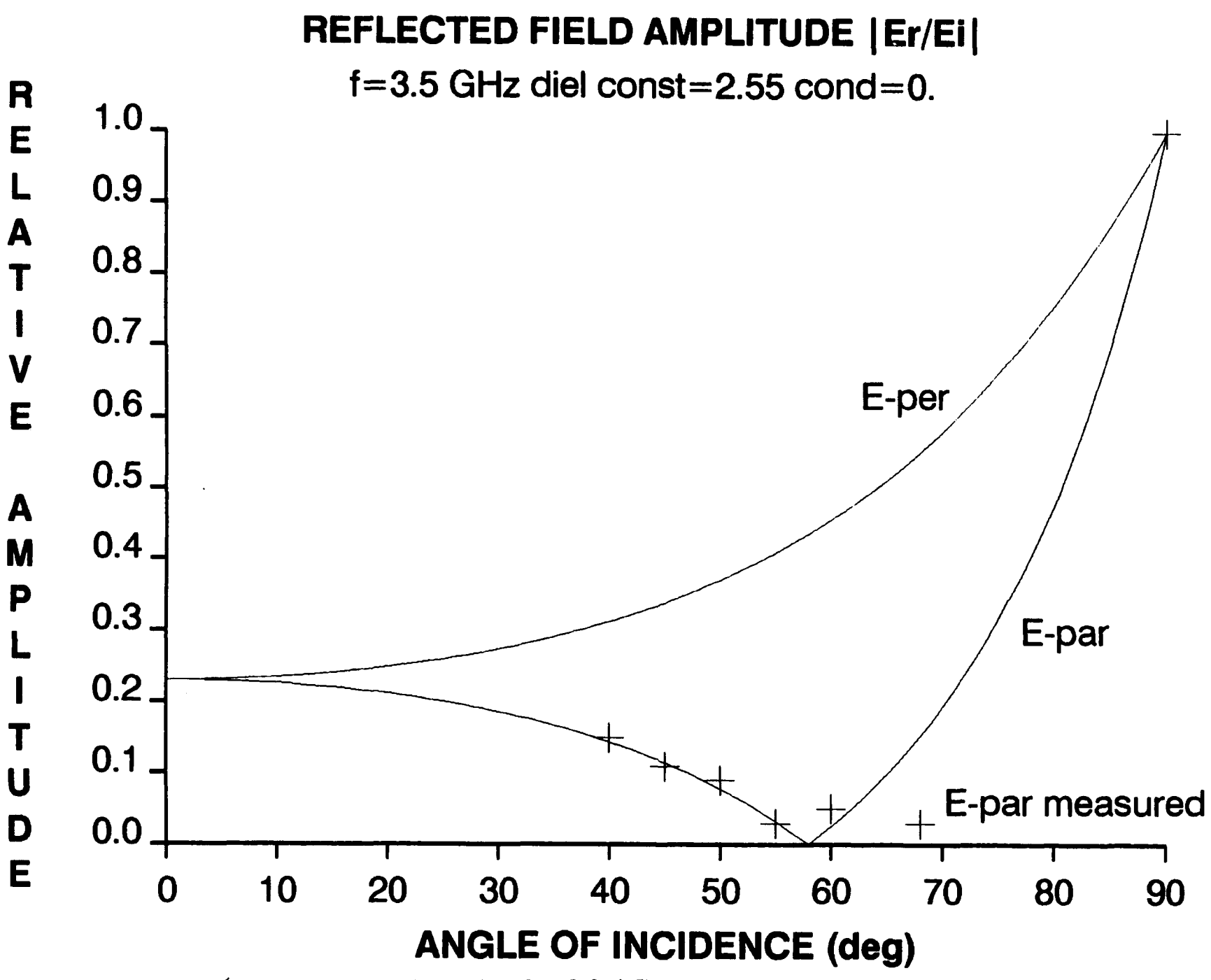

Fig. 6. Reflected field amplitude, f=3.5 GHz.

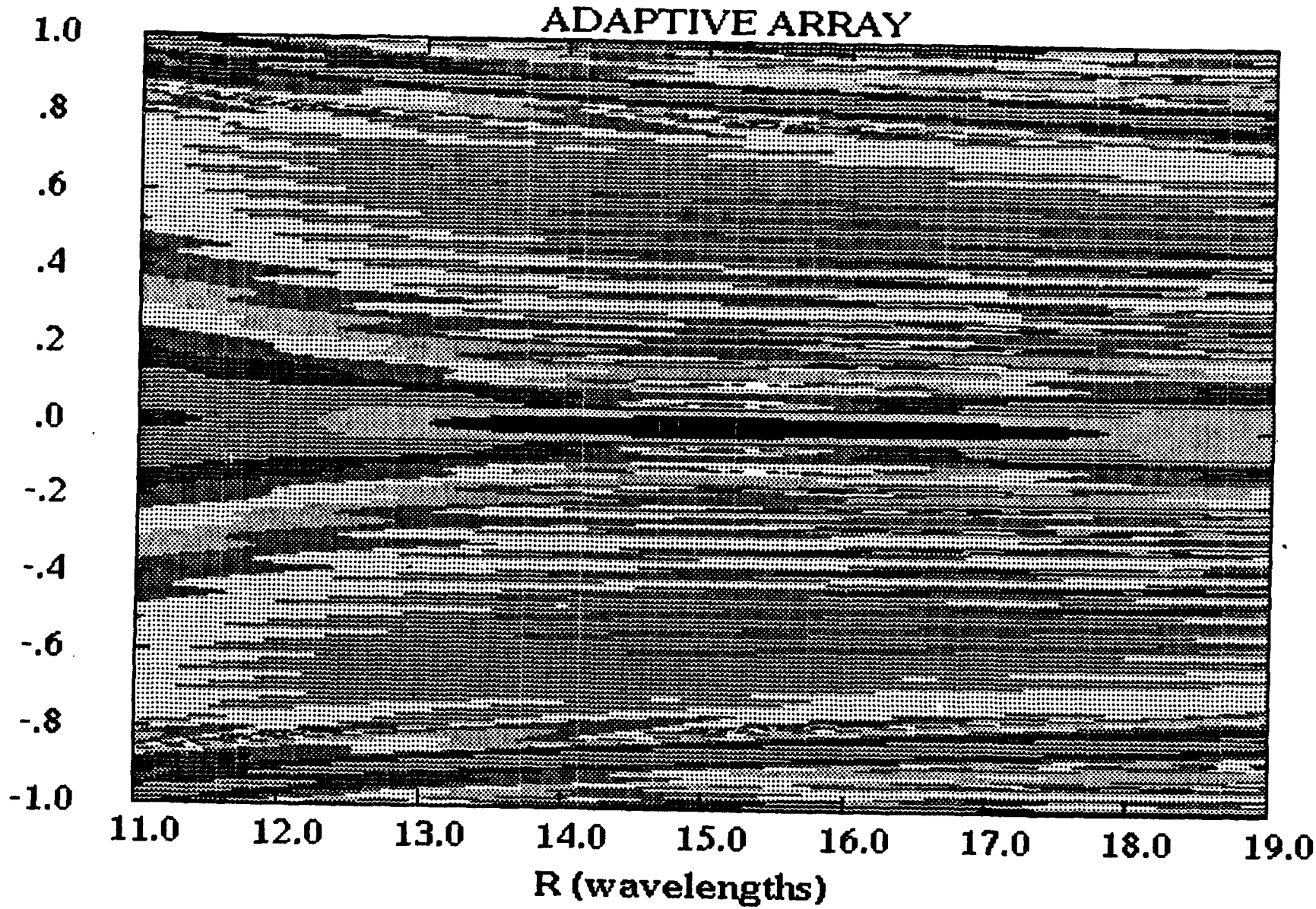

Fig. 7. Near-field pattern of focused array.

in a dry sand medium having zero conductivity and a dielectric constant of 2.55. Superimposed on the parallel polarization curve are measured data points at several angles of incidence using two antennas in a configuration similar to the proposed one, showing good agreement with the theoretical curve. The large reduction in reflection amplitude in an angular region about the Brewster angle is evident, showing that a large range of oblique angles will significantly reduce surface reflections. Such a range of oblique angles would occur in the angles to the elements in a receiving array. Fig. 5 shows similar results for an L-band frequency of 1.55 GHz in the sand medium with a 10% water content giving it a dielectric constant of 4.0 and a conductivity of .073. Here it is seen that there is an analogue to the Brewster angle in a conductive medium where there is still a large reduction in surface reflections. This effect is observed in the oblique incidence of radio waves on the sea surface. The measured data is also shown.

Fig. 9 shows a y-z plane image of the reflections from dry sand taken at the Brewster angle with the 22 element y-collinear line array illustrated in Fig. 8 and Fig. 11 is the image of a metal mine. These can be compared with the corresponding images taken at vertical incidence in Figs. 13 and 14. In the former case, the mine-to-soil reflection intensity ratio is 43.8 while the vertical incidence case decreases it to 6.77. Over an 8 dB increase in signal-to-clutter ratio is obtained through the use of oblique forward scattering at the Brewster angle.

3.3 Buried Anti-tank Mine Reflection Characteristics

Buried mine forward scattering measurements were done in dry and moist sand for fixed angle of incidence and varying mine depth. A summary of some of the results is given in Table 1. The ratio of the signal-to-clutter of the mine reflection to the soil reflection is given as S/C. The M15 metal mine has an expected high forward scattering level at both frequencies. The plastic M19 has a lower return but would still be detectable, especially when

FOCUSED ARRAY GPR IMAGING
IMAGING EXPERIMENT

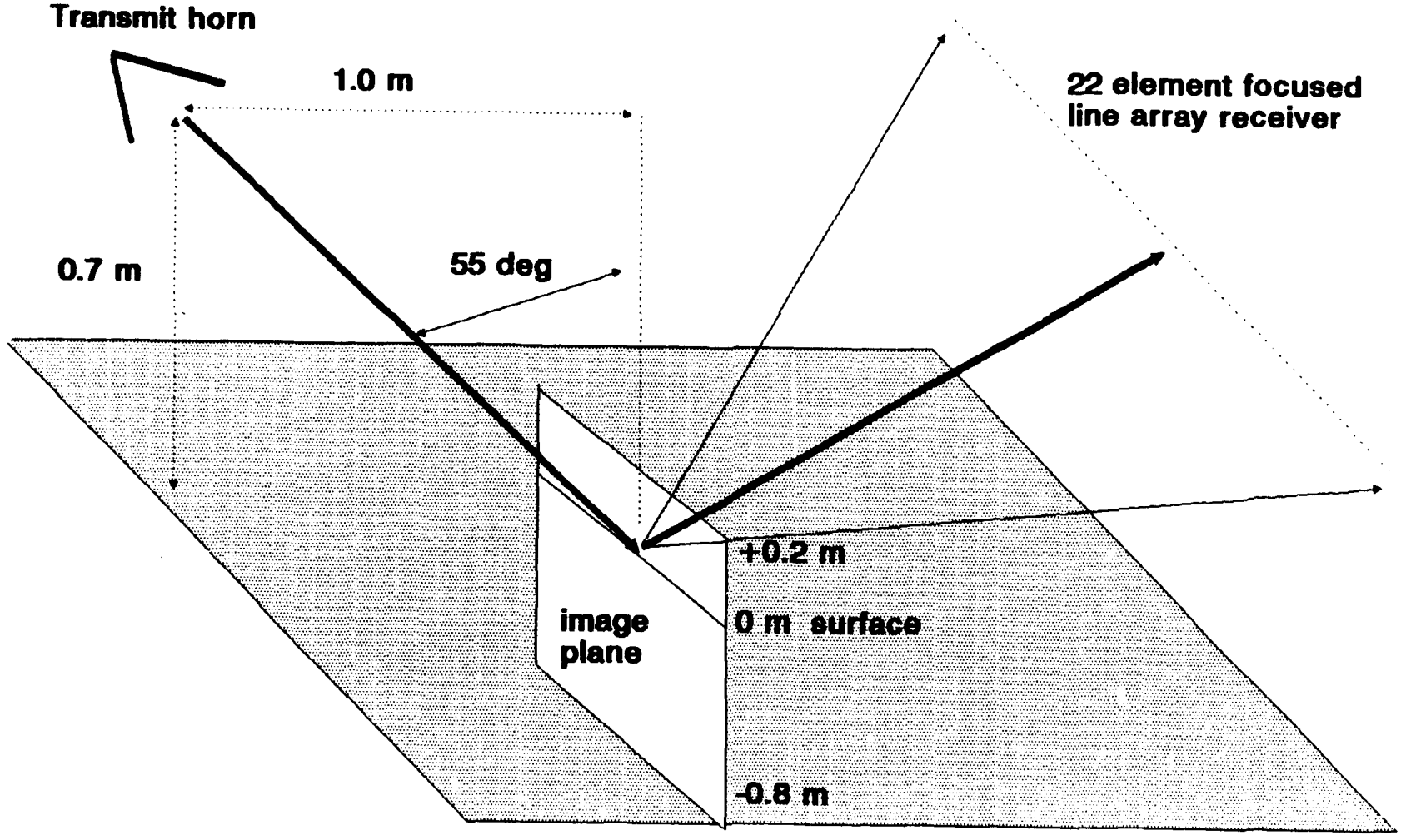

Fig. 8. Horizontal line array experimental system.

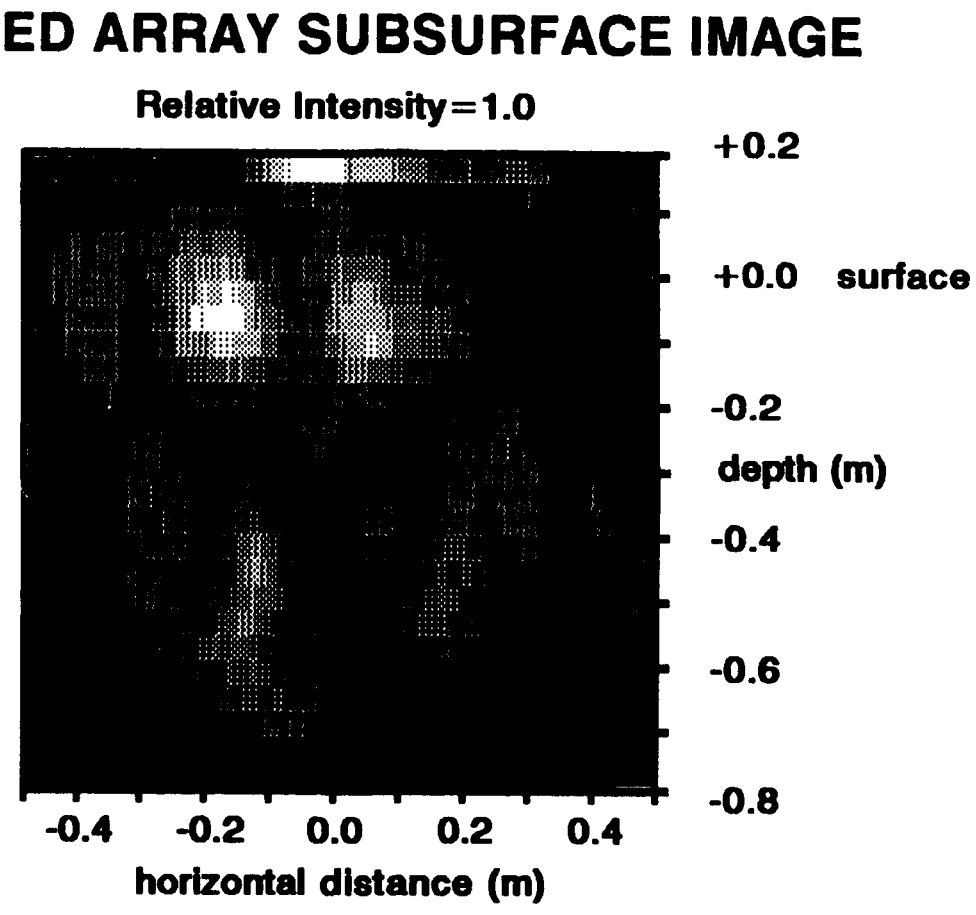

Fig. 9. Subsurface yz-plane image, y array, ground surface.

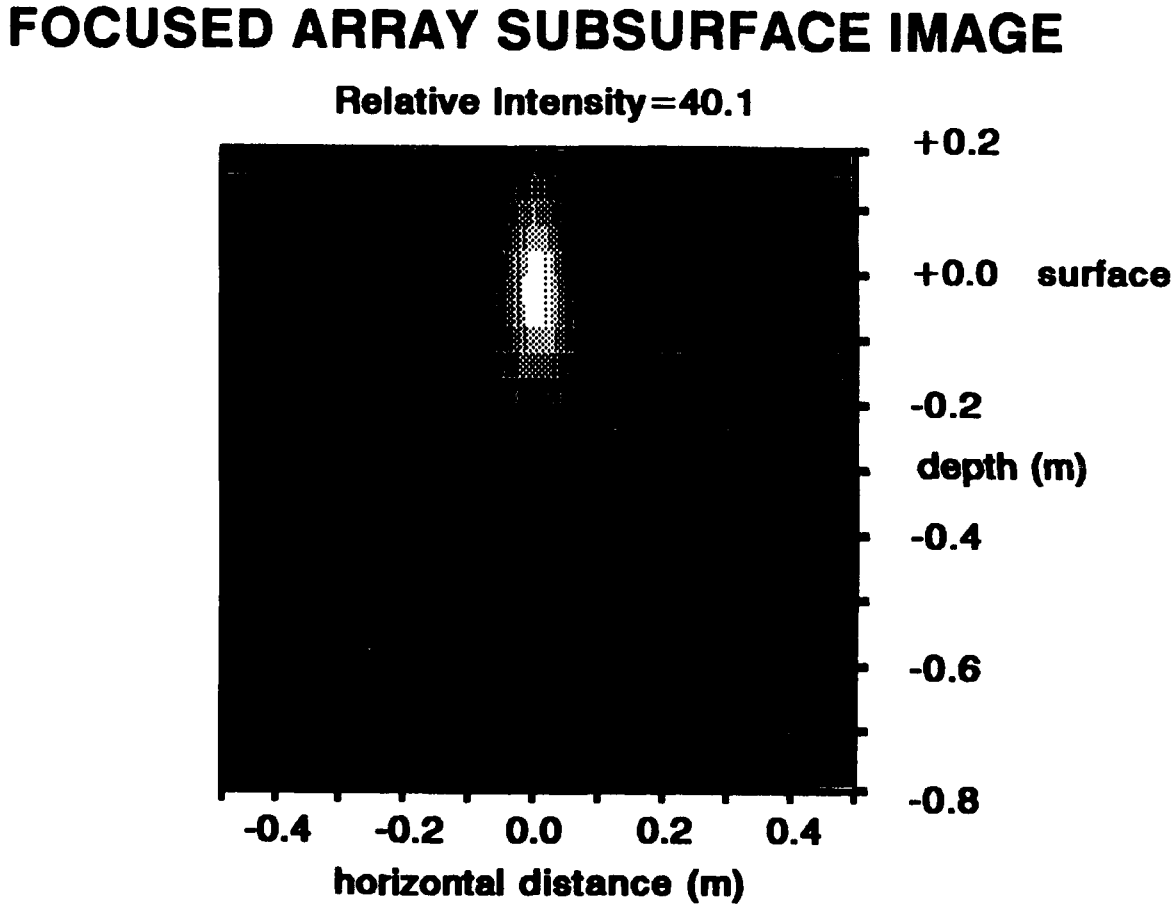

Fig. 10. Subsurface yz-plane image, y array, metal ruler.

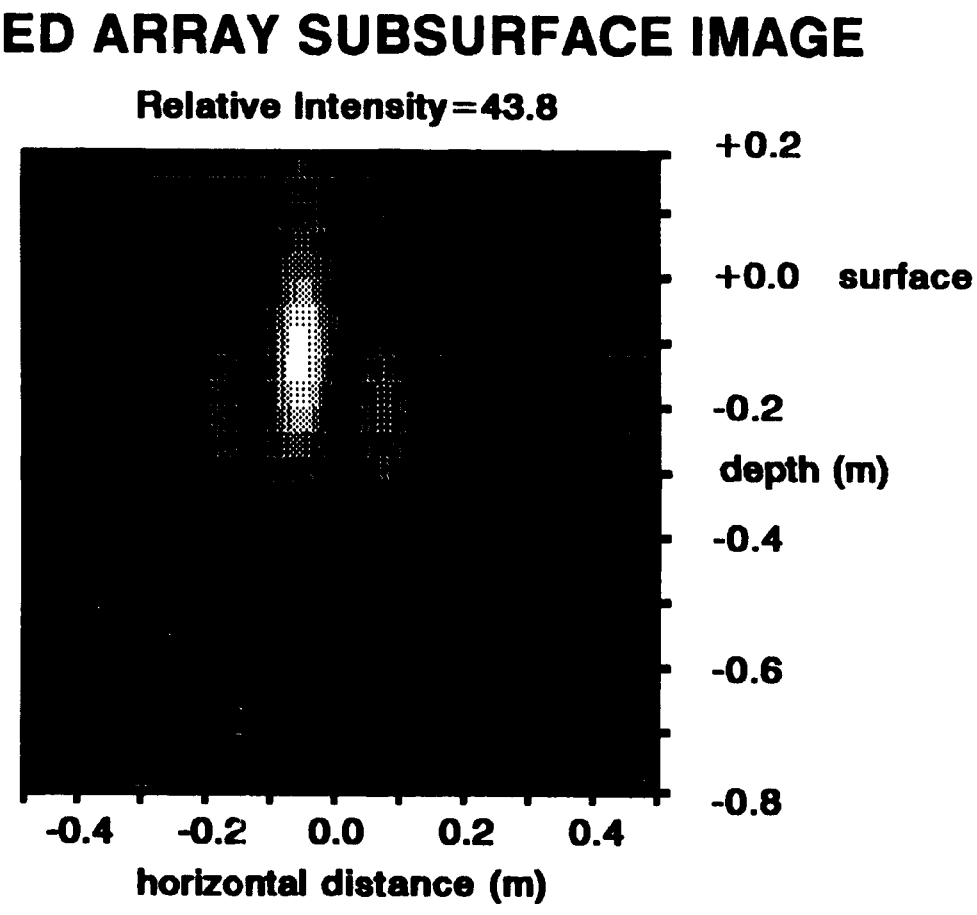

Fig. 11. Subsurface yz-plane image, y array, M15 metal mine.

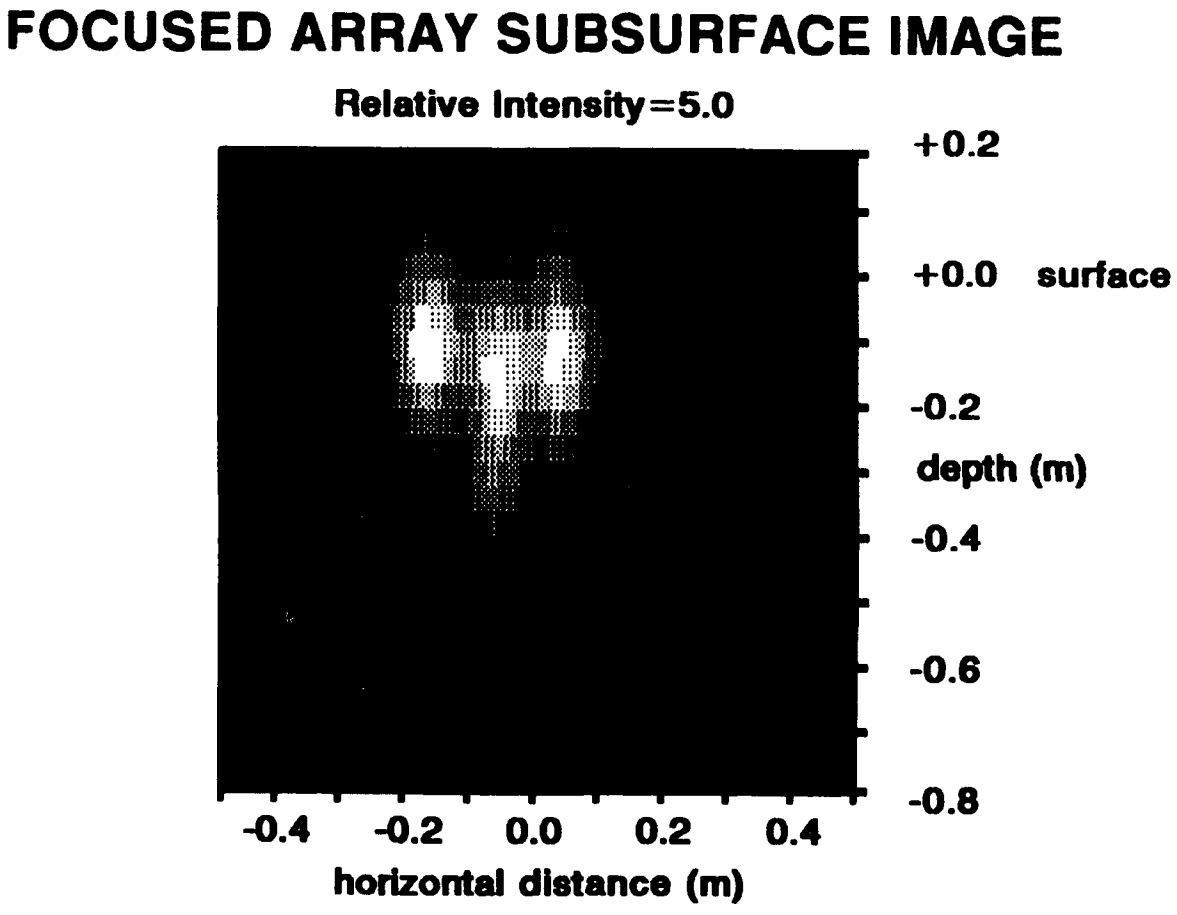

Fig. 12. Subsurface yz-plane image, y array, M19 plastic mine.

Table 1. Peak Reflection Levels

L-Band (1.55 GHz) 0% water

Mine	R	AOI	d	S/C
M15	1.8m	45 deg	5.0 cm	12 dB
M19	1.8m	45 deg	7.5 cm	5 dB

S-Band (3.5 GHz) 0% water

Mine	R	AOI	d	S/C
M15	1.2m	55 deg	3.8 cm	20 dB
M19	1.2m	55 deg	3.5 cm	5 dB

S-Band (3.5 GHz) 10% water

Mine	R	AOI	d	S/C
M19	1.2m	55 deg	3.8 cm	4 dB

An important advantage of the proposed system is the potential ability to obtain mine shape and signature information for classification of mine type. In our previous work, one-dimensional focused array measurements of buried anti-tank mines were done using a forward scattering horizontal line array. The I and Q outputs for each array element were sampled, and the array was then digitally focused and scanned to form the images. Experiments were done using a 16 element L-band array and a 22 element S-band array. The array response results show detectability of both metal and plastic buried mines at L-band but no shape information because of the long wavelength (20 cm). In contrast, the S-band array data shows a distinct variation in level while scanning over the surfaces of both metal M15 and plastic M19 buried mines. This is an initial demonstration of the ability to obtain shape information for buried mines at S-band frequencies.

These S-band measurements of anti-tank mines buried in sand were made using a bistatic S-band radar system having a wide beam standard gain horn as

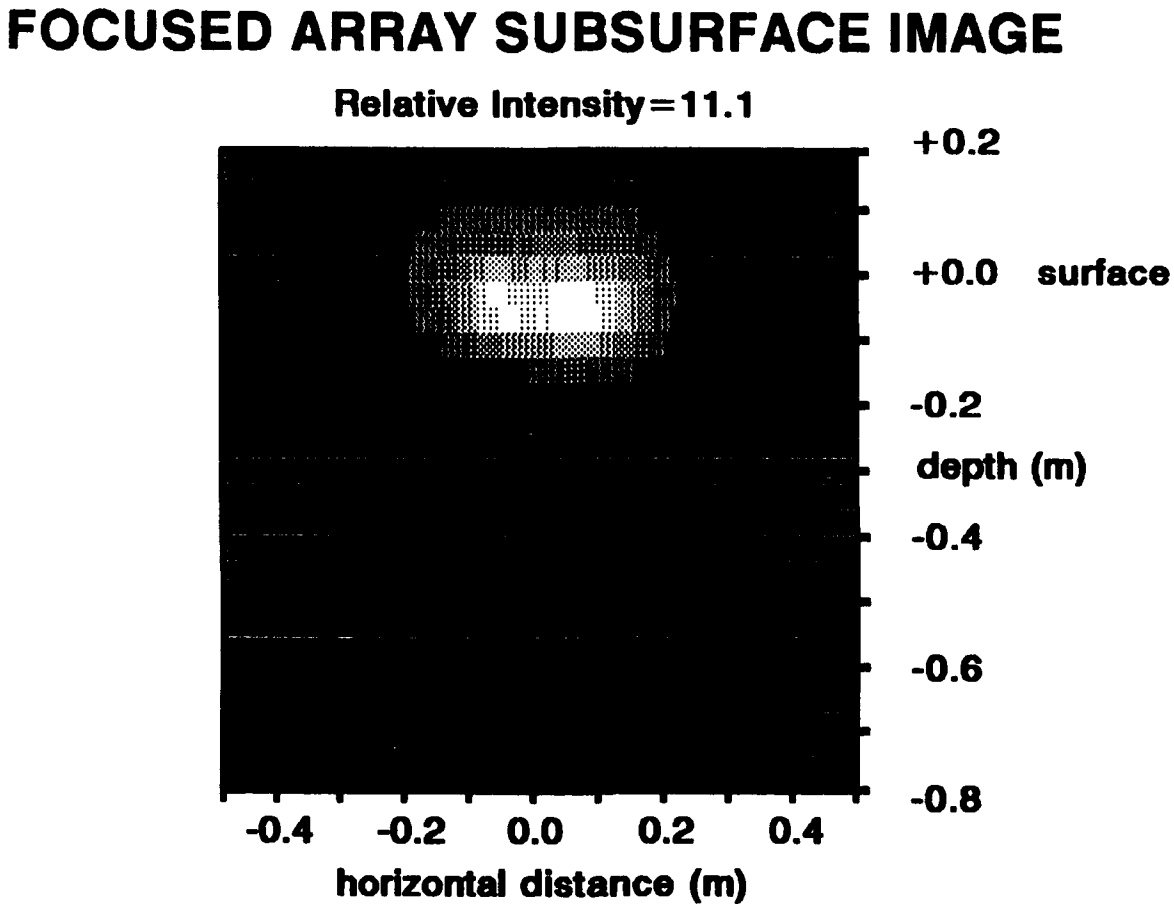

Fig. 13. Subsurface yz-plane image, y array, ground, vertical incidence.

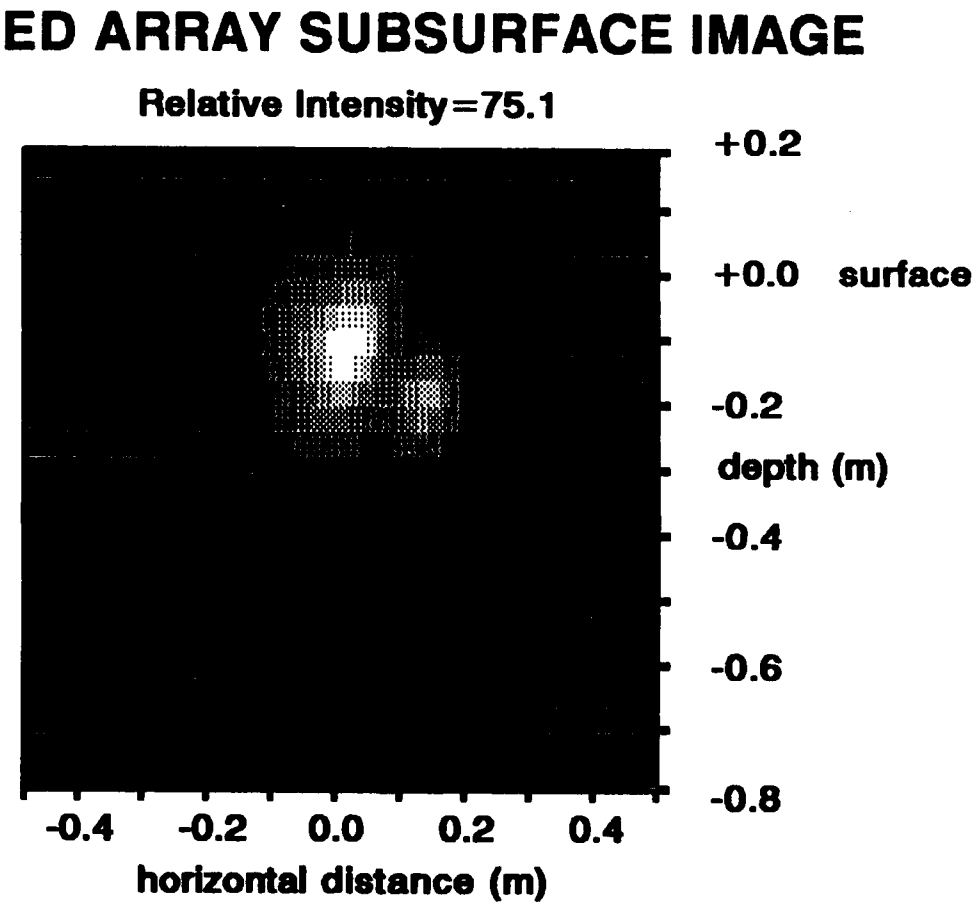

Fig. 14. Subsurface yz-plane image, y array, M15, vertical incidence.

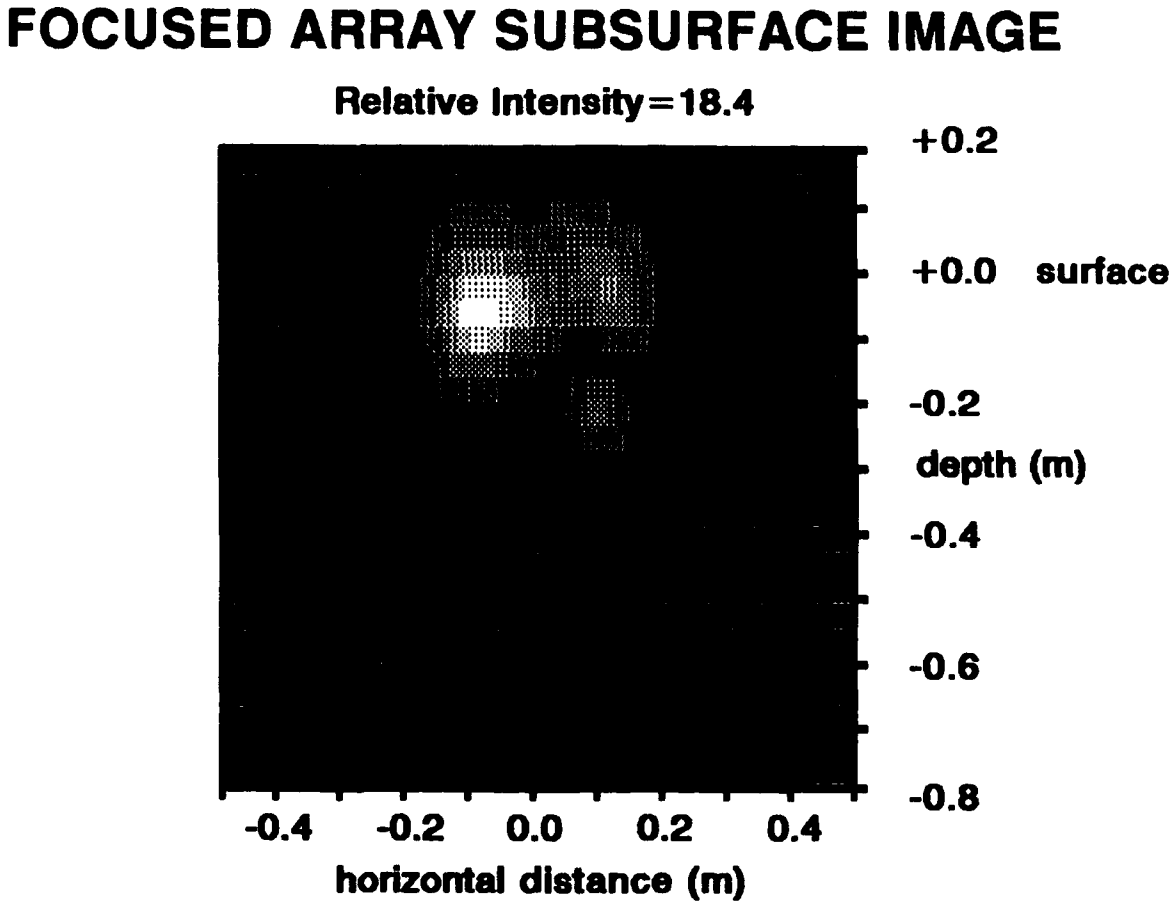

Fig. 15. Subsurface yz-plane image, y array, M19, vertical incidence.

ing antenna, as illustrated in Fig. 8. The system used the oblique forward scattering geometry with the transmit and receive antennas at the 55 degree Brewster angles of incidence and reflection, respectively. The antennas were at a height above the sand surface of .7 m with a separation of 2.0 m. The targets were individually located centrally between the transmit and receive antennas, and baseband I and Q element data was sampled by a 20 GHz HP 54120T sampling oscilloscope. Focused array digital beamforming was then done in the y dimension with focusing depth as a parameter. The array was scanned to 100 points in y (transverse horizontal) over a 1 m distance, at each of 25 focal depths in 4 cm increments varying from .2 m above the surface of the ground to .8 m below the surface. The resulting data was then converted to power, quantized into 16 levels, and a half-tone gray-level image was generated for each target with power decreasing from white to black.

Fig. 10 is an image of a 1 in x 12 in metal ruler on the ground surface oriented with its long side in the plane of incidence, i. e., the x-z plane, perpendicular to the direction of the horizontal line array. The resolution in the y direction indicated by the image is about 5 cm which agrees with the theoretically predicted value.

The image of Fig. 11 is that of an M15 metal mine buried at a depth of 7.5 cm and normalized to its peak. In this image, there is notable detail across the mine horizontal dimension with the largest reflection from the raised central pressure plate and two secondary reflection lobes from the annulus surrounding the pressure plate. The highest image intensity also occurs at the correct depth of 7.5 cm. Some smearing of the image occurs above the surface since the depth of field is large enough to capture some of the very high reflections from the mine surface even while it is focused above the ground. This phenomenon will not occur with weaker targets, such as the M19 plastic mine also at a depth of 7.5 cm, shown in Fig. 12. Detail is apparent across the mine surface, with lobes at the top sides of the mine. The peak again occurs at the actual mine depth.

These images show that both metal and plastic buried mines can be detected and shape information can be obtained using a high resolution array at S-band with bistatic oblique forward scattering near the Brewster angle. The images also show that the signatures of the two mines are different and also

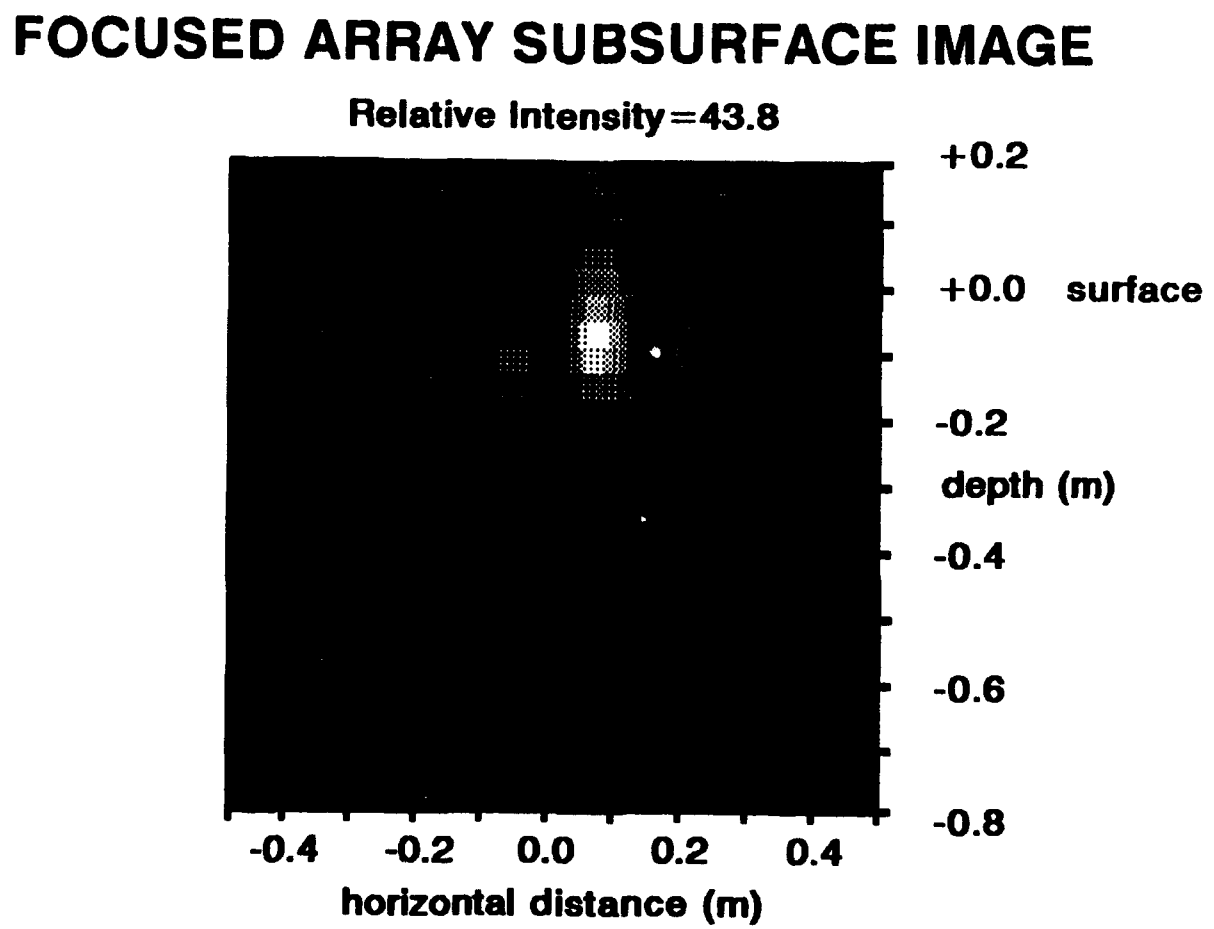

Fig. 16. Subsurface yz-plane image, y array, M15, refraction included.

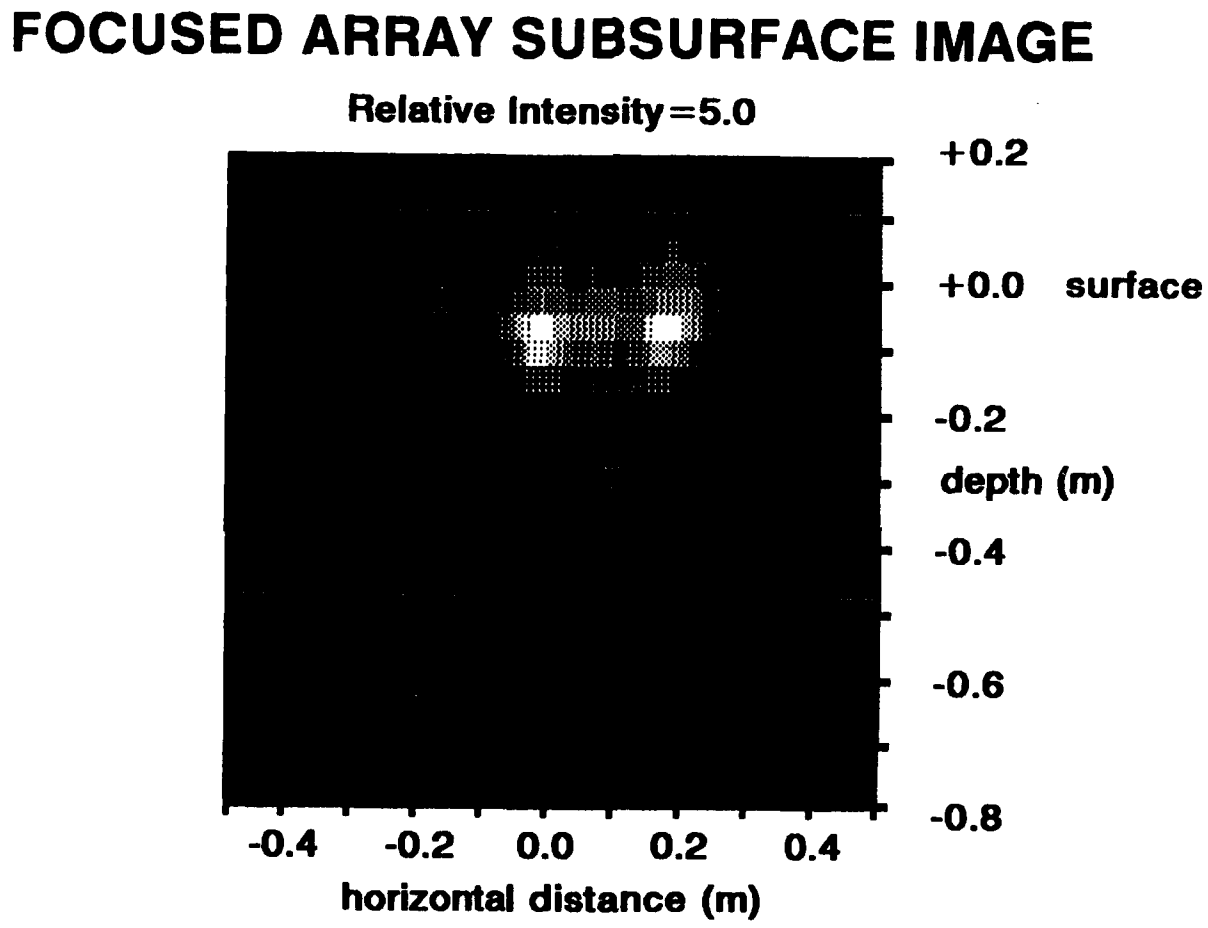

Fig. 17. Subsurface yz-plane image, y array, M19, refraction included.

ture. The results show that the proposed system using a rectangular focused array formed by synthetic aperture to obtain two-dimensional surface shape information has a high probability of success.

3.4 Effect of Refraction

The mine scattering images were modified by the addition of a phase correction for the medium refraction. The effects were shown in Section 2.4. The images show that the refraction effect should be included even for shallow mines since the depth resolution is improved as seen in Figs. 16 and 17.

4.0 EXPERIMENTAL RESULTS

4.1 Objective

The purpose of the Phase I experiment was to provide some information on the capabilities of a rectangular focused array using the Brewster angle propagation geometry (oblique bistatic scattering). The proposed system design and the Phase II experiment both will use a horizontal line array perpendicular to the direction of forward motion at the Brewster angle of reflection, which receives the scattered radiation from a target illuminated by a transmitter at the Brewster angle of incidence. As the entire system moves in the forward direction, a rectangular array is formed by synthetic aperture techniques using sequential forward positions of the horizontal line array.

The Phase I experiment was set up to demonstrate some of the three-dimensional detection and imaging capabilities of the proposed system without actually using a filled synthetic rectangular array. The experiment used two orthogonal synthetic line arrays, one in the x-direction and one in the y-direction as illustrated in Fig. 18. These arrays were synthesized by using a single antenna which was moved to 22 element positions to form each line array. This allowed the Phase I experiment to be performed at very low cost. The Phase II experiment will use a complete horizontal line array of 32 individual antennas, with the forward motion of the array synthetically forming a rectangular array. The y-array provided the image and resolution character-

PHASE I EXPERIMENT CONFIGURATION

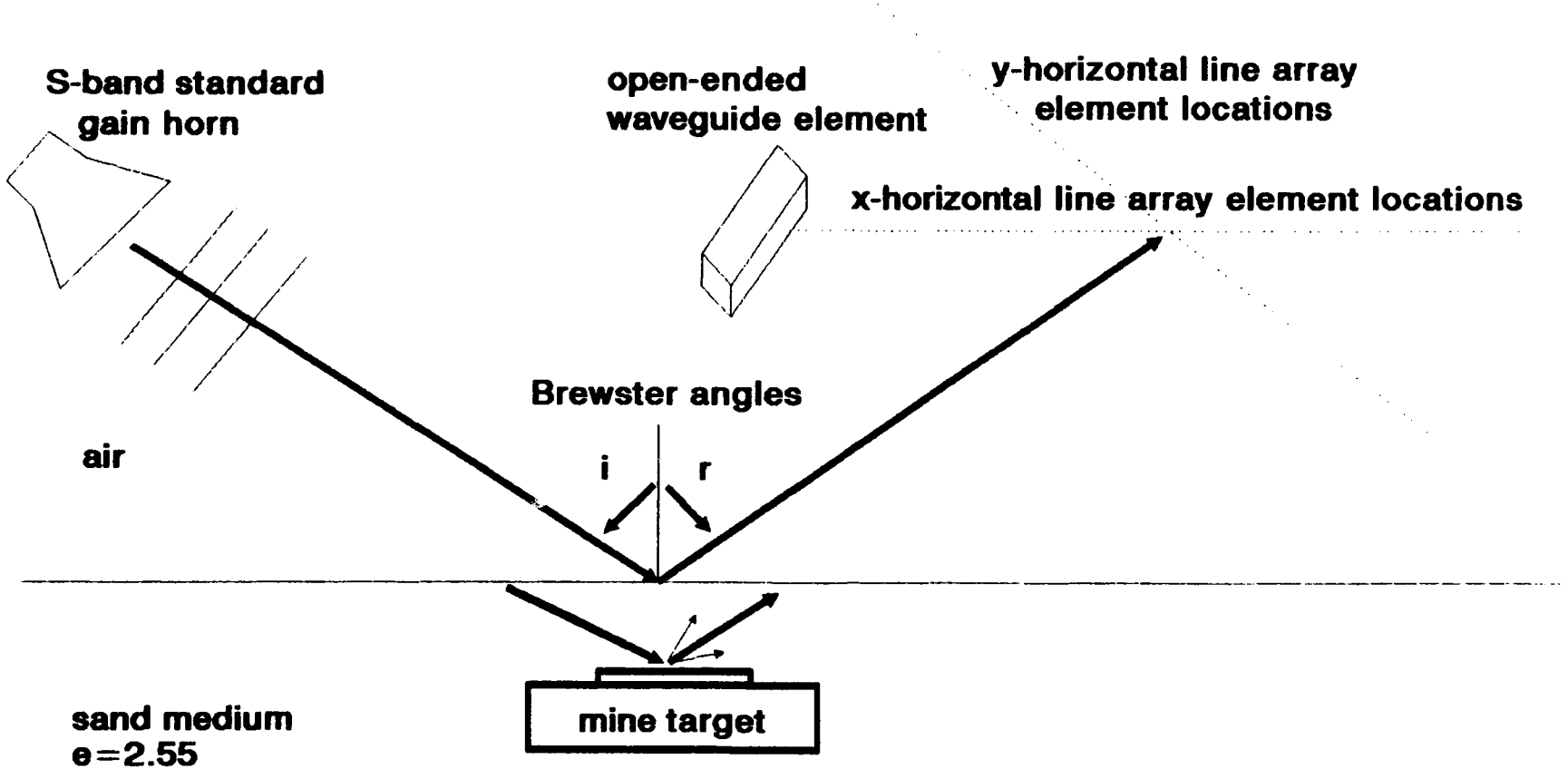

Fig. 18. Phase I experimental configuration.

the x-z plane characteristics. Combining the x and y arrays into a crossed line array configuration was used to form an image in the x-y plane. In the actual proposed system, all three image planes would be provided by a single filled rectangular array.

4.2 Hardware and Software Design

The experiment was performed using two crossed orthogonal line arrays as the receiver and an S-band standard gain horn antenna as the transmitter at a frequency of 3.5 GHz, as illustrated in Fig. 18. A photograph of the experimental setup is given in Fig. 21. The transmit antenna and receiver array were separated by 2 m at a height of .7 m, with the mine targets at the center at a depth of 7.5 cm. The arrays were synthetically formed by moving a single open-ended waveguide antenna to 22 element locations equally spaced by one wavelength of 8.57 cm, in each of the line arrays oriented along the x and y axes. The combination of the two line arrays was also used to form a 44 element cross array. These synthetic array measurements were made for a metal ruler reference, the sand surface, a metal M15 AT mine, and a plastic M19 AT mine.

The arrays could be focused and scanned over any of three orthogonal planes at any location. The developed software properly corrects for the dielectric constant and conductivity of the soil so that refraction correction is properly included. Images can be formed in any of the three orthogonal planes at any position in the field of view.

The waveform used was a one nanosecond pulse at the frequency of 3.5 GHz. This allowed the elimination of the direct path leakage from transmitter directly to the receiver by time gating. Quadrature mixers in the receiver generated baseband I and Q components, which were individually sampled and stored for each element position by an HP54120T 20 GHz sampling oscilloscope. At the received pulse peak, one sample from each of the I and Q waveforms was used as the input to the beamforming algorithm. This procedure in effect simulated a CW source at the frequency of 3.5 GHz. The experimental system diagram is given in Fig. 19 and the transmitter and receiver module is shown in Fig. 20.

PHASE I EXPERIMENTAL SYSTEM

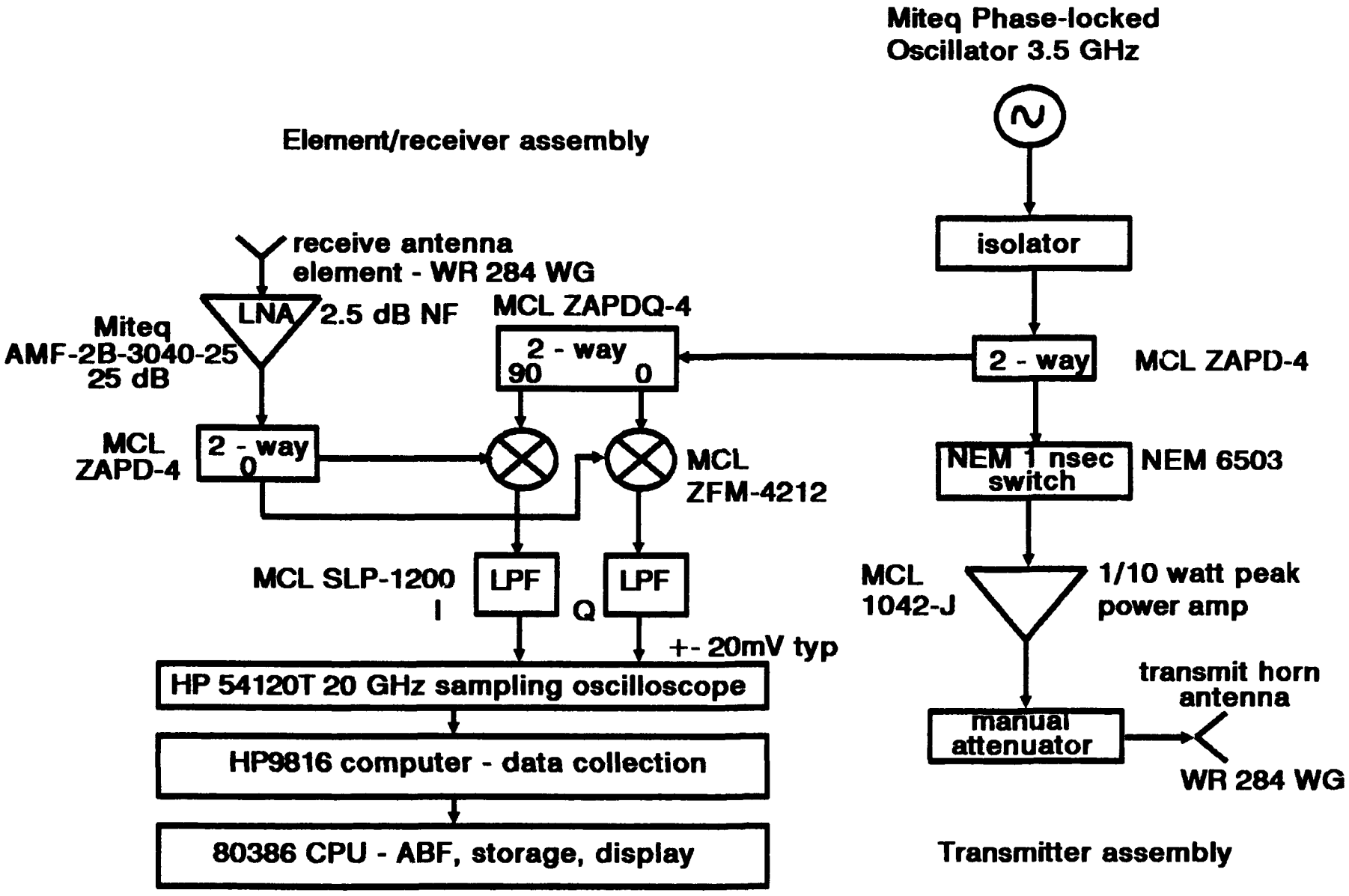

Fig. 19. Phase I experimental system diagram.

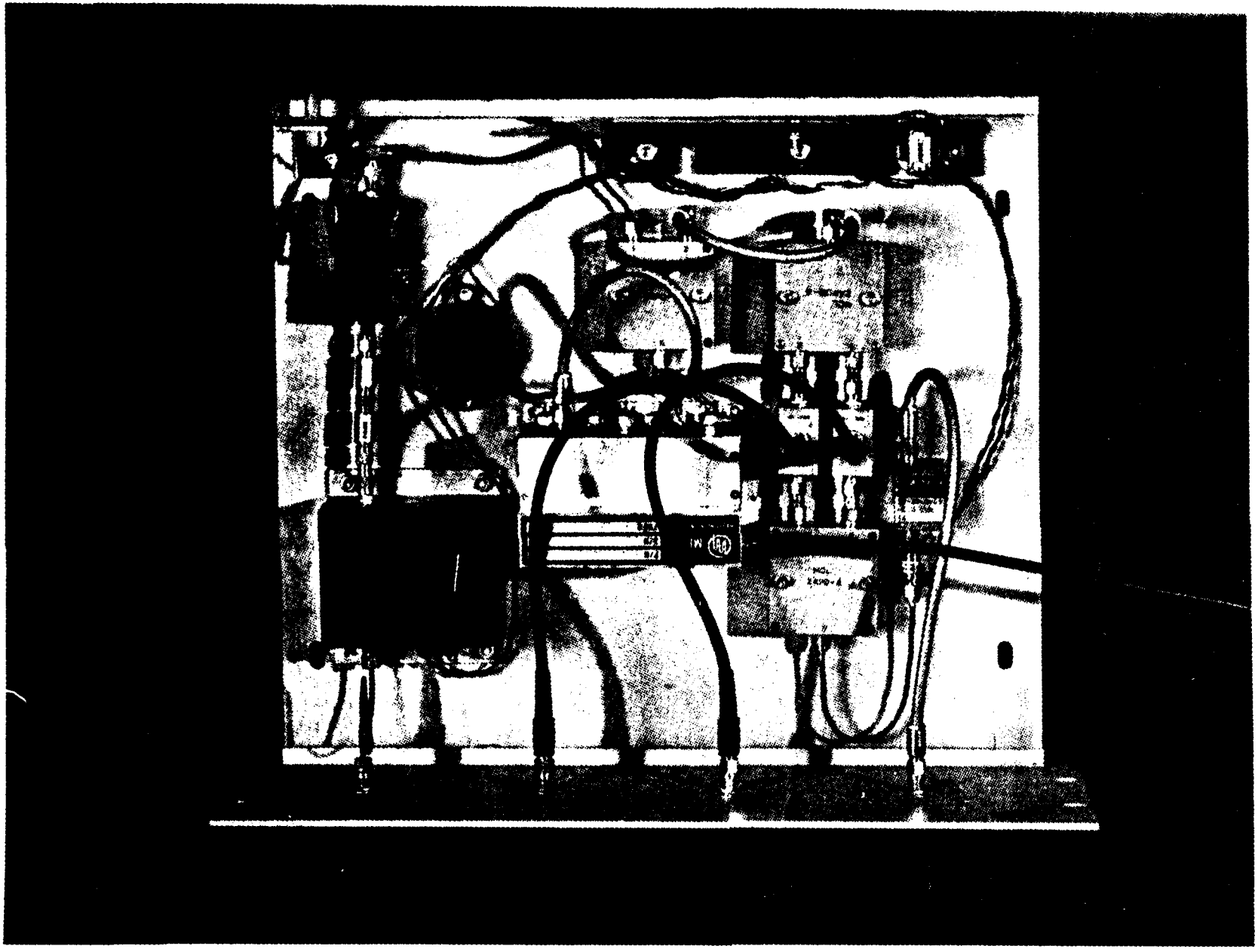

Fig. 20. Phase I experimental system transmitter and receiver module.

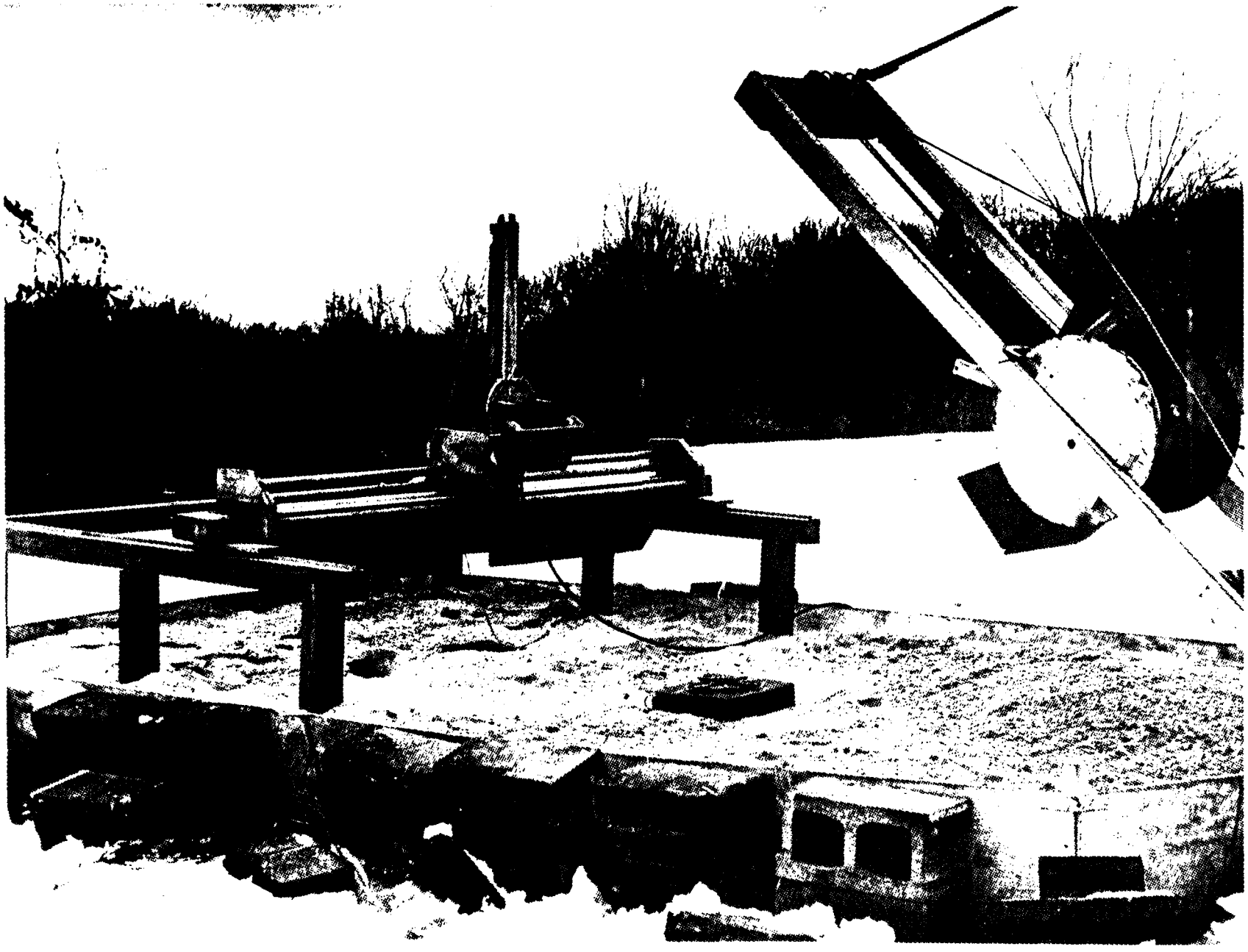

Fig. 21. Phase I experimental mine detection facility.

4.3 Results

The results of the experiments allowed positive detection and identification of both plastic and metal mines by providing high resolution three-dimensional images of the mines. Furthermore, no interference from surface reflections is evident in the images indicating a successful reduction or elimination of these reflections by the Brewster angle propagation geometry.

A difficulty in using the crossed line array configuration to simulate a filled rectangular array is the conical beam of each of the component line arrays which causes an undesirable spreading of the signal due to the high sidelobes when the arrays are combined. Since this effect would not exist with a complete rectangular array, some of the images were filtered with a spatial and lower amplitude cutoff to eliminate the spreading.

In order to approximate the resolution of the proposed rectangular array, the resolution of the x-array was measured in the x direction by forming an image of the metal ruler now oriented parallel to the y axis. The image was made in the x-z plane and is shown in Fig. 26 indicating the resolution in the x and z directions. The x resolution is about 5 cm, while the z resolution is about 16 cm. This image can be compared with that of Fig. 10 which is the image of the metal ruler parallel to the x-axis measured with the y-array giving the y and z resolution of the y-array.

Images of the mines were then made using the 22 element x-array and y-array separately, and the 44 element crossed line array combination of the x and y arrays as illustrated in Fig. 18. The images from the x-array are in the x-z plane (side view) through the center of the mine (y=0), while the images using the y-array are in the y-z plane (front view) through the center of the target (x=101.6 cm) as illustrated in Fig. 8. The images using the crossed line array are in the x-y plane (top view) at the mine depth (z=7.5 cm). The relative intensity, which is proportional to power, has been quantized into eight gray levels from white to black in descending intensity, with each image normalized to its own peak. The images cover a 1 meter square area centered on the target location. The origin of the coordinate system for the image graphs was on the ground surface above the center of the target location in the array coordinate system (101.6,0,0).

FOCUSED ARRAY SUBSURFACE IMAGE

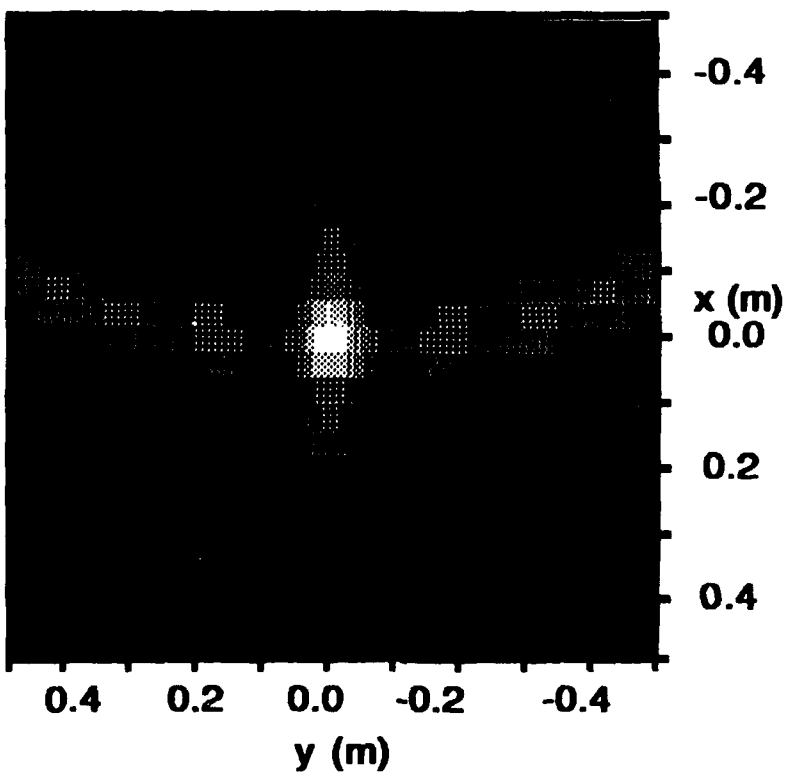

Fig. 22. 2-D response in horizontal plane of focused x-y crossed arrays.

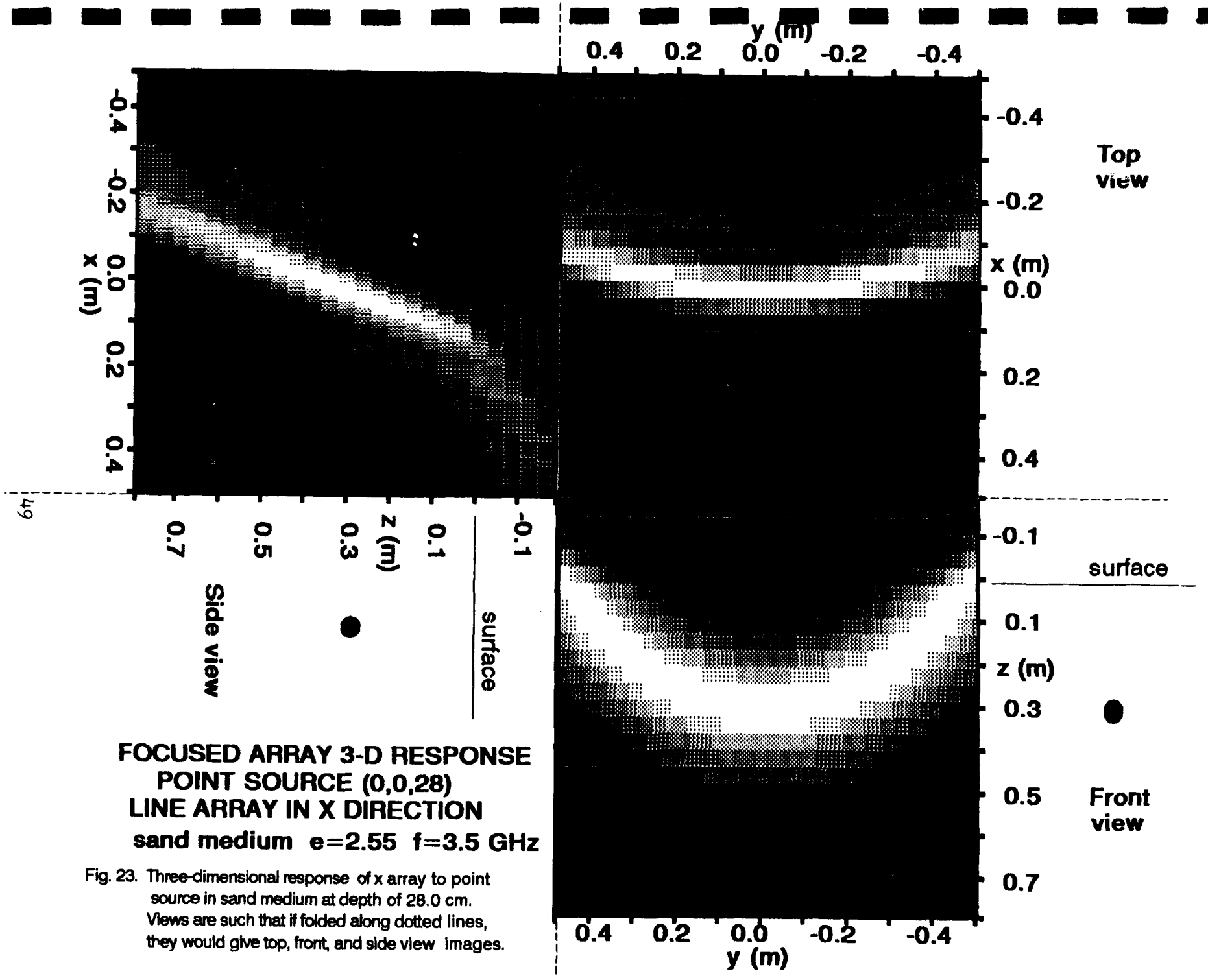

FOCUSED ARRAY 3-D RESPONSE
POINT SOURCE (0,0,28)
LINE ARRAY IN X DIRECTION
sand medium e=2.55 f=3.5 GHz

Fig. 23. Three-dimensional response of x array to point source in sand medium at depth of 28.0 cm. Views are such that if folded along dotted lines, they would give top, front, and side view images.

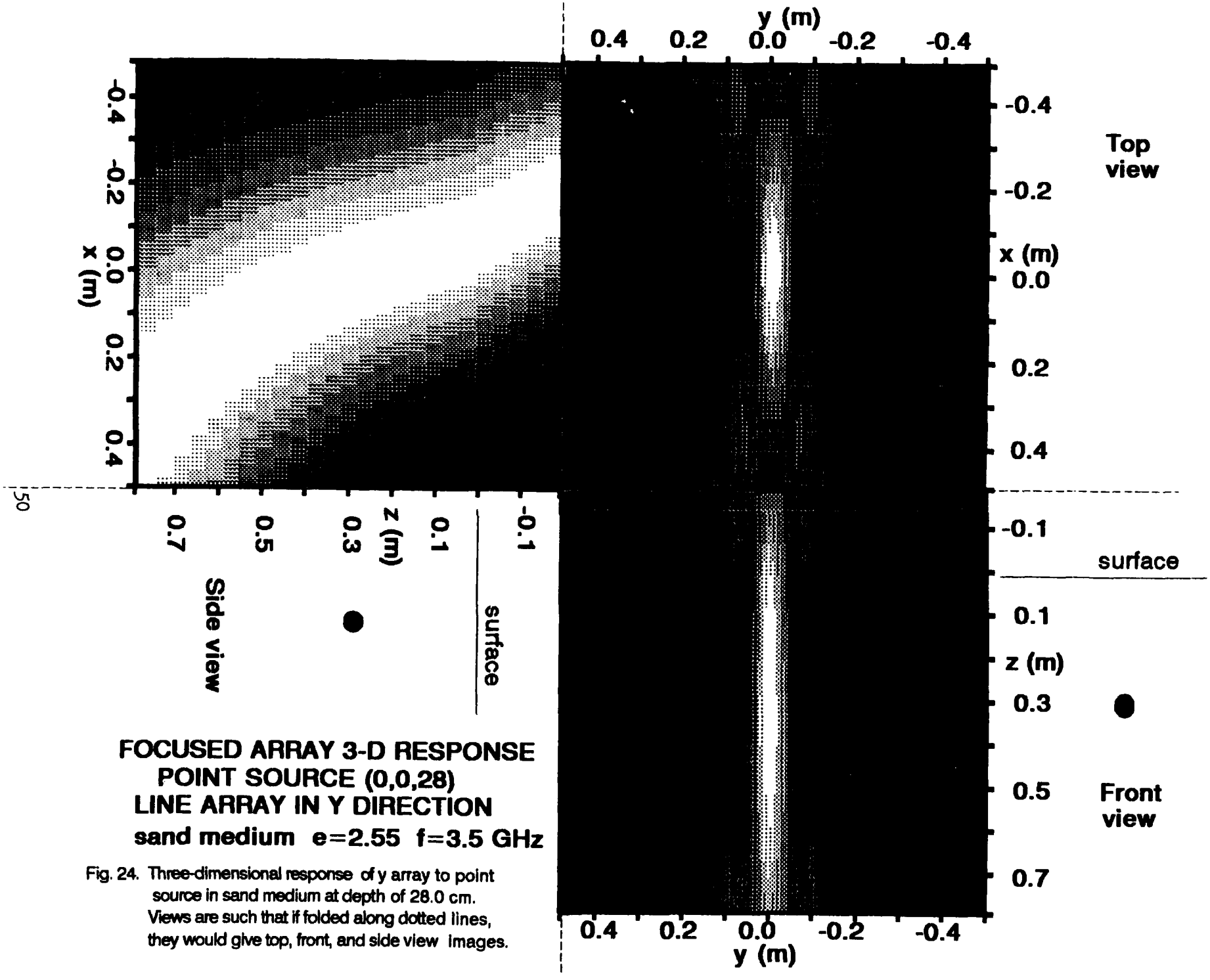

Fig. 24. Three-dimensional response of y array to point source in sand medium at depth of 28.0 cm. Views are such that if folded along dotted lines, they would give top, front, and side view images.

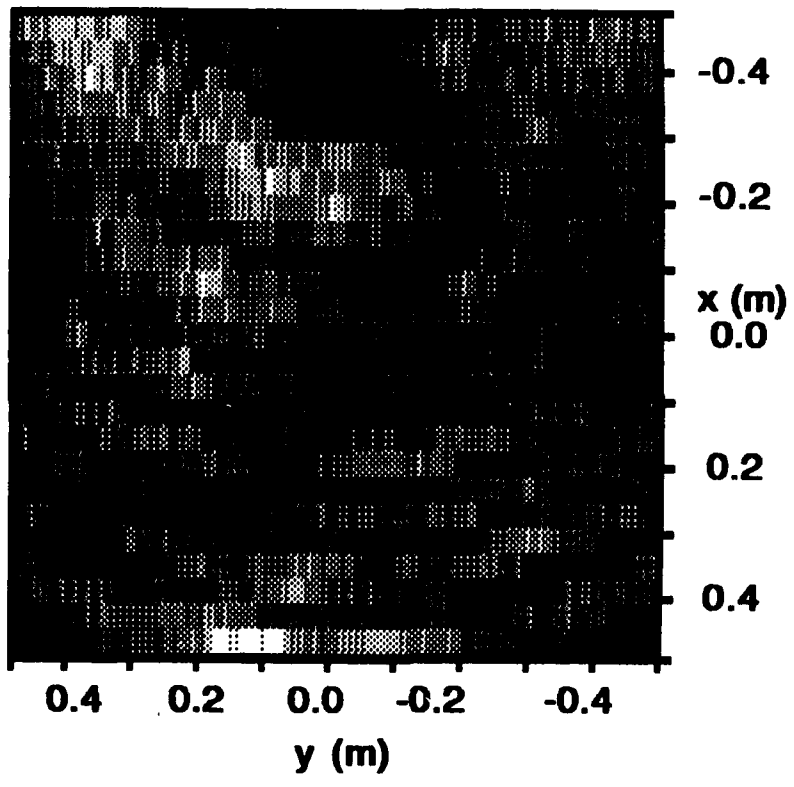

Fig. 25. Subsurface xy-plane image, x-y crossed arrays, ground surface.

FOCUSED ARRAY SUBSURFACE IMAGE

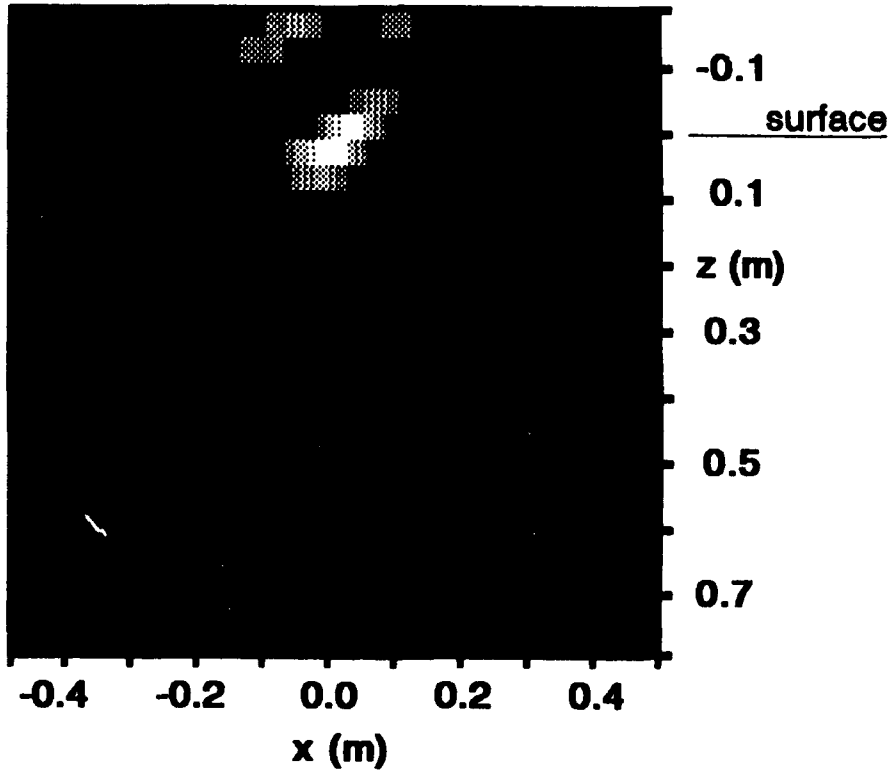

Fig. 26. Subsurface xz-plane image, x array, metal ruler.

x-y plane using the crossed line arrays in the absence of any targets. The peak voltage received is 21 mv and the scattering is roughly uniform over the image area.

4.3.1 Focused Array 3-D Images of Metal M15 Anti-Tank Mine

The first target was an M15 metal anti-tank mine. The mine is approximately cylindrical with a diameter of 31.8 cm and a center height of 7.3 cm. The mine was buried with its top at a depth of z = 7.5 cm below the sand surface. Images were made in the three orthogonal planes as described above to approximate the images which would be obtained with the proposed focused synthetic rectangular array. The medium was dry sand with a dielectric constant of 2.55 and conductivity of 0.

The three orthogonal image planes are presented in Fig. 27 in a format which allows easy visualization of the three-dimensional characteristics of the image. Each of the views, top, front, and side, is accompanied by a profile of the mine geometry in that aspect, drawn to scale, and in the proper location with respect to the vertical axis of the image graph. The x and y axes are centered on the mine target center, while the origin of the z axis is at the ground surface, which is indicated above the mine diagram in the front and side views. The three views are oriented such that if the side and front view images were folded down, together with the top view they would form half of a cube giving a three-dimensional mine image formed by projections on the sides of the cube.

The top view image measured with the x-y crossed line array configuration is of the x-y plane at the target depth of z = 7.5 cm. The peak array output voltage is 307 mv, which is 23.3 dB above the sand surface reflection shown in Fig. 25. The top view image of the metal mine also shows a very distinctive scattering pattern, with the peak scattering from the 19 cm diameter top pressure plate, shown as the inner concentric circle in the mine profile diagram. Dual secondary scattering points are seen at the edge of the mine on the transmitter side at the top of the image. Another secondary scattering point is seen at the annulus on the receiver side. The image has been spatially filtered in the y direction to eliminate the effects of the high

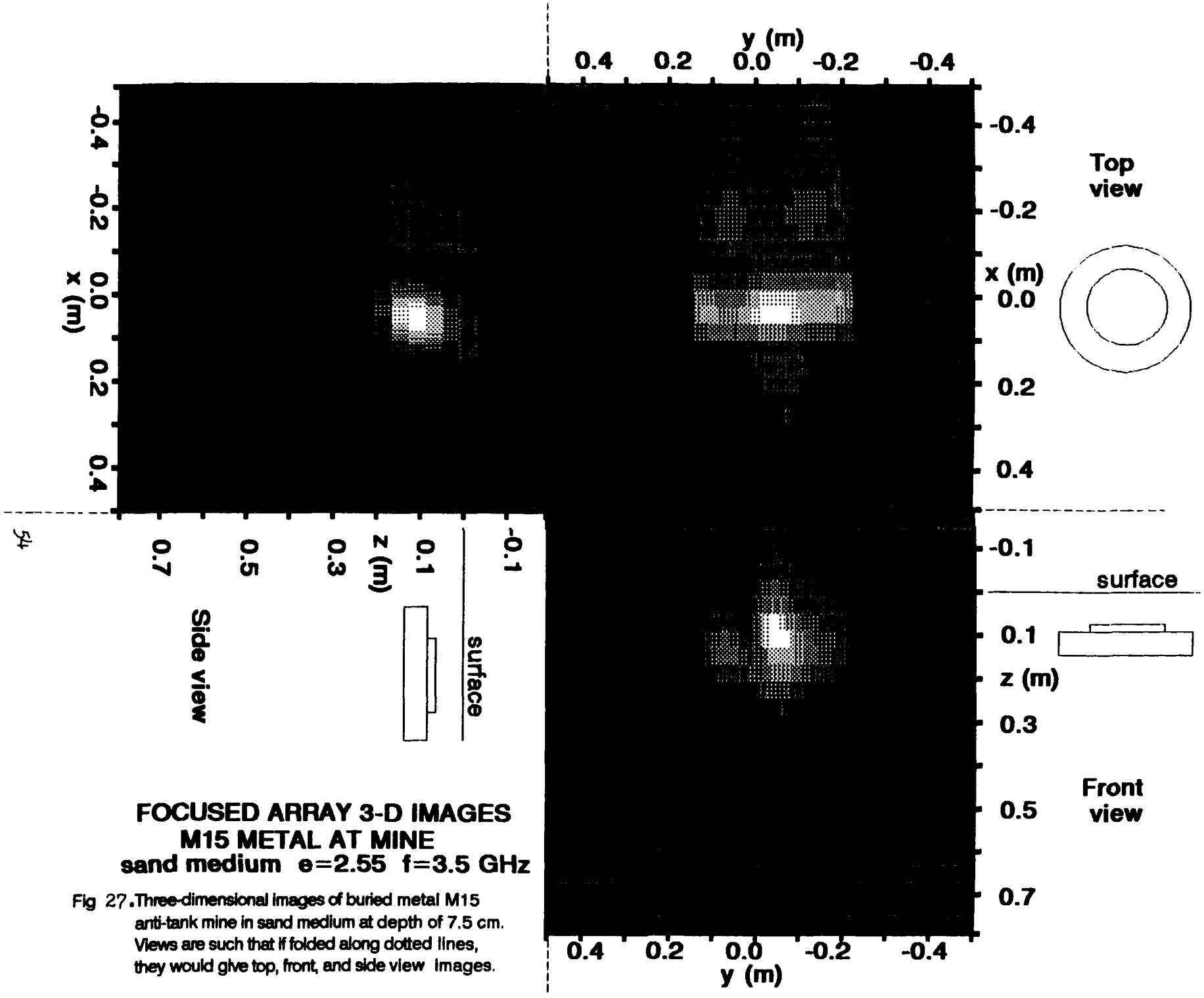

54

FOCUSED ARRAY 3-D IMAGES
M15 METAL AT MINE
sand medium e=2.55 f=3.5 GHz

Fig 27. Three-dimensional images of buried metal M15 anti-tank mine in sand medium at depth of 7.5 cm. Views are such that if folded along dotted lines, they would give top, front, and side view images.

array.

The front view image was measured with the y-array and shows the y-z plane with the mine profile and ground surface indicated. The image shows the maximum reflection at the mine depth of 7.5 cm, with the image width corresponding well with the actual mine diameter. At the mine depth of 7.5 cm, the image intensity corresponds with a projection of the top view image on to the y-z plane at x = 0. The vertical extent of the image is increased because of the depth of field of the y array.

The side view image was measured with the x-oriented array, and is an image in the x-z plane. The mine profile and ground surface are also indicated. The maximum image intensity corresponds well with the mine depth, and there is also good correspondence with a projection of the x-y plane image on to the x-z plane at the target depth of 7.5 cm. If the image is viewed as a projection, the correspondence can be clearly seen with the peak reflection from the top pressure plate and the secondary reflection from the transmitter side of the mine in the top view image.

This composite three-dimensional image or any of its component plane images, combined with the peak image intensity would provide positive identification of the M15 metal mine. Because of the detail seen in the three-dimensional scattering pattern, it is expected that different types of mines of different composition will give very different and characteristic scattering signatures. Also the x,y and z localization of the mine is very accurate, giving the location of the mine correctly to within 4 cm in any coordinate.

4.3.2 Focused Array 3-D Images of Plastic M19 Anti-Tank Mine

Focused array measurements were also made of an M19 plastic anti-tank mine. The top of the mine is square, 33.0 cm on a side, and it has a center height of 8.9 cm to the top of the pressure plate, which is 25.4 cm in diameter. The composition of the pressure plate is bakelite (phenol formaldehyde) which has a dielectric constant of 3.70 at the frequency of 3.5 GHz. The mine was inert so it contained no explosive material. Below the top pressure plate is a significant air gap, followed by more plastic, and in a real mine there would be the primer. The actual refraction and scattering mechanism is too

complex to understand without a detailed electromagnetic analysis, but the primary contributor to the mine scattering is believed to be the air gap through a complex relationship with the soil, pressure plate, and other parts of the mine. The presence of explosive material in the mine may also affect the scattering characteristics.

The images of Fig. 28 show the three orthogonal plane views of the M19 plastic mine buried with its top at a depth of 7.5 cm. The top view is an image of the x-y plane at the 7.5 cm depth. The peak voltage is 89 mv, which is 12.5 dB higher than the peak sand surface reflection so that the surface reflection is below the lowest quantization level in the image. The image shows a distinctive scattering pattern with primary scattering points located on the left and right of the top mine surface, and little or no scattering from the top center. The maximum x and y dimensions of the image correspond exactly with the dimensions of the mine. This image has also been spatially filtered and a lower amplitude cutoff has been used to eliminate the effects of the high sidelobes caused by the conical beam of the x array.

The front view of the mine shows the y-z plane image measured with the y array. This image also shows the dual scattering points on the left and right of the mine. The peak amplitude occurs at the depth of 7.5 cm. Also, the front view image gives a good indication of the vertical dimension of the mine and the y-dimension of the image corresponds well with the width of the mine. The y-z image can be seen to be a projection of the x-y plane image.

The side view image is of the x-z plane and was measured with the x array. It also has its maximum at the actual depth and x position of the mine. This image has been spatially filtered in the z dimension to eliminate the artifacts caused by the conical beam of the x array.

The location and dimensions of the mine can be accurately obtained from these images, although the x-y plane image taken with the crossed line arrays is sufficient for detection, identification, and localization. The front and side view images add to an understanding of how a focused rectangular array would perform, and the imaging characteristics of the array in three dimensions. The three-dimensional images also give a greater understanding of the scattering characteristics of the mines with the proposed system.

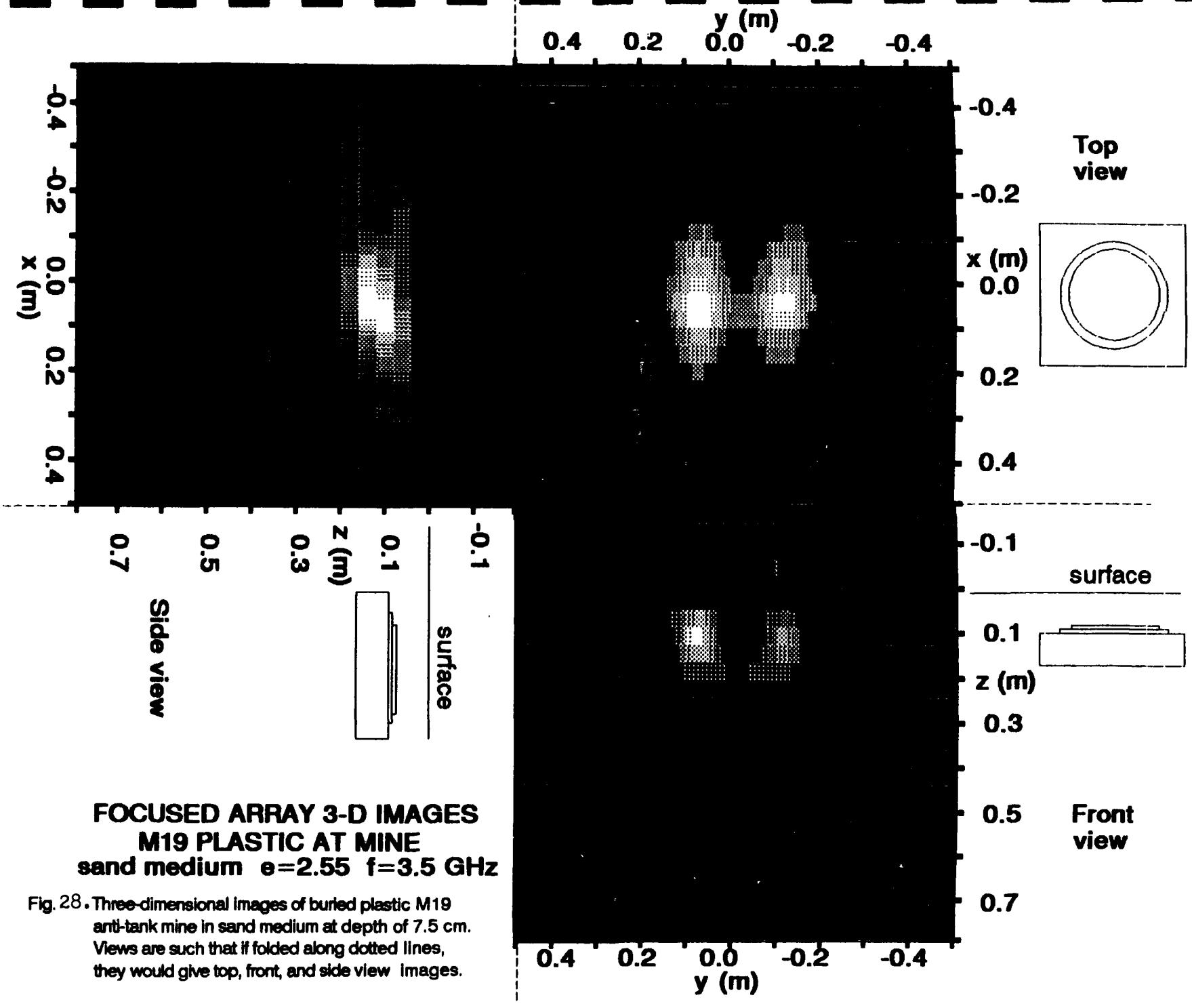

FOCUSED ARRAY 3-D IMAGES
M19 PLASTIC AT MINE
sand medium e=2.55 f=3.5 GHz

Fig. 28. Three-dimensional images of buried plastic M19 anti-tank mine in sand medium at depth of 7.5 cm. Views are such that if folded along dotted lines, they would give top, front, and side view images.

4.4 Conclusions

These results demonstrate the resolution and detection capability of a two-dimensional rectangular focused synthetic array, even though the experiments have used a much simplified array consisting of two 22 element crossed line arrays. A filled rectangular array of 32 x 32 elements would enhance the detectability by approximately 10*log(1024/44) = 13.7 dB. The addition of the synthetic array in the x direction has improved the resolution in the x dimension to 5 cm. The images taken have shown that this is sufficient to both detect and identify by characteristic signatures both metal and plastic anti-tank mines.

A high resolution three-dimensional imaging capability has been demonstrated, which provides shape information of a mine indirectly through an interpretation of its scattering pattern seen in the image. These images are characteristic signatures of various types of mines, and must be studied and catalogued in order to be used for mine identification. However it is the very complexity and detail of these images due to the high resolution, which makes them valuable and easy to distinguish from other buried objects.

The hardware used a 1 nsec pulse to gate out the direct path signal from transmitter to receiver. This broadband pulse would exhibit serious dispersion effects in moist soil. Because of this all of the measurements were performed in dry sand. Measurements in moist soil must use a narrow band pulse or continuous wave radiation. The effects of moist soil would be an increased attenuation of the subsurface signal, a change in the mine reflection level because of the increase in the dielectric constant of the soil, and a change in the soil reflection characteristics caused by the dielectric constant and non-zero conductivity. However, the results shown in Fig. 5 have indicated that a Brewster angle type of effect also exists in moist soil, so that a large reduction in surface reflections would still be achieved in moist soil using the proposed Brewster angle propagation geometry. The Phase II experiments will also test the system in soil of varying moisture content.

The Phase II experiments should include AT mine simulants which accurately simulate the physical characteristics of the mine including explosive content.

It is concluded from the results of these experiments that the proposed system concept can achieve the performance of 5 cm resolution, detection of metal and plastic mines, three-dimensional imaging, and mine characterization and identification through characteristic signatures

5.0 FOCUSED ARRAY SYSTEM DESIGN

The objective of this task was to develop a conceptual system design of the proposed focused rectangular synthetic array sufficient to determine feasibility of the technique. This was carried one step further by developing a system design that not only would satisfy the performance requirements, but could also be fabricated and tested in a simplified form during the Phase II program.

The optimum frequency of the system appears to be S-band, since good resolution is obtained and attenuation is acceptable even in moist soils at the shallow depths expected for anti-tank mines. However, frequencies as high as C-band in the 5-6 GHz range may still be acceptable if attenuation is not too high, and the resolution will be increased proportionately.

Although the Phase I experiments used a 1 nsec pulse to reduce the direct path signal from transmitter to receiver, this is only appropriate in a non-conducting medium because of frequency dispersion. In moist soil, a short pulse would become highly distorted from this dispersion. Since the array is focused, it has a depth of field which gives it axial resolution, so a pulse is not needed. Since it is desirable to use FFT digital beamforming to form the beams from the horizontal array, a CW waveform will be used. This has the additional major advantage of no bandwidth requirements on the system components. Reduction of any direct path signal components can be achieved by simply placing an absorbing microwave barrier in the line of sight between transmitter and receiver where it will not interfere with the ground reflected signals.

The system design has incorporated some major simplifications which eliminate practically all constraints on speed of forward motion. One of these is the method of beamforming which uses mathematical simplifications to separate the beamforming in the x and y directions, reducing the beamforming

computations at each forward position to an easily manageable number. Another is the use of FFT digital beamforming for the 32 focused beams from the horizontal array at each image position.

5.1 Focused Synthetic Array System Geometry

The focused rectangular synthetic array system concept is presented in Fig. 1. The system geometry has been chosen to be the same as the previous experimental geometry with antenna heights of 70.12 cm and separation of 203.2 cm. The desired field of view is chosen to be the ground surface area defined by the length of the receiver array in one dimension and the transmit-receive antenna separation in the other. The intercepted angle of this area in the plane of incidence through the center of the array is 70.96 degrees. In order to achieve more uniform illumination of the ground surface area, the antenna axes should be pointed at 35.48 degrees.

The actual 3 dB coverage area depends upon both the transmit and receive antenna patterns and the 1/R variation of the field to different points in the coverage area. Considering all these factors, the actual 3 dB coverage area is 1.25 m lateral by 1.524 m longitudinal, centered on the ground midpoint of the system which has the maximum illumination level. This coverage will give a direct path level from transmit to receive antennas of -8.91 dB, which should be further reduced by microwave absorber placed in the line of sight of the antennas at a height of 35.06 cm so that it does not obstruct the ground reflected path.

5.2 Antennas

It is desirable to have a transmit antenna which gives a uniform illumination of a large field of view so that a large receive array can be formed. The first type of antenna considered for the transmitter was simply an unfocused line array which would illuminate the ground in its near-field. It was believed that this would give a uniform illumination out to the horizontal extent of the system. However this was found to be unsatisfactory since the computed near field was found to oscillate over a range of 3dB or more which

would seriously affect the uniformity of illumination and, consequently, the image. An array would also be much more complex to design and fabricate.

A much better and simpler solution was found to be the use of a tapered horn antenna, whose beam taper would be tailored to the desired field of view of the system. To achieve the optimum illumination as shown in Fig. 40 would require a horn fed by standard WR284 waveguide. The horn would be flared only in the E-plane, since the WR284 H-plane dimension of a=2.84 in gives a 3 dB beamwidth of about 63 degrees in the horizontal. The horn would be flared in the E-plane to give a vertical dimension of b=2.5585 in.

Figs. 29 is the H-plane pattern of the horn antenna as a function of azimuth angle. Fig. 30 is the corresponding E-plane pattern vs. vertical angle.

The receiver array is a 32 element array of half-wave dipoles. The scan limit of this array is arbitrarily chosen to be the ground projection of the array. For this distance, the maximum scan angle is 40.18 degrees. Far-field arrays exhibit a grating lobe equal in amplitude to the main beam when the beam is scanned beyond a critical angle which depends upon the array element spacing. A near-field focused array will exhibit a pseudo-grating lobe because of incomplete constructive interference, which has a large increase in amplitude, but is less than the main beam. In order to avoid a pseudo-grating lobe at the opposite edge of the field of view at 40.18 degrees, the element spacing must be no greater than 0.775 wavelengths. This indicates an array length of 24.8 wavelengths, or 2.1254 meters.

The H-plane pattern of this array focused at the ground surface at the midway point between transmitter and receiver is shown in Fig. 31. Fig. 32 is the pattern when the array is scanned to the edge of the field of view showing the pseudo grating lobe which appears at the opposite edge of the field of view.

5.3 Transmitter and Receiver

Fabrication of the receiver array would be simple, since beamforming would be digital and no power combination would be necessary. Each element has a coherent quadrature phase comparator and dual A/D converters.

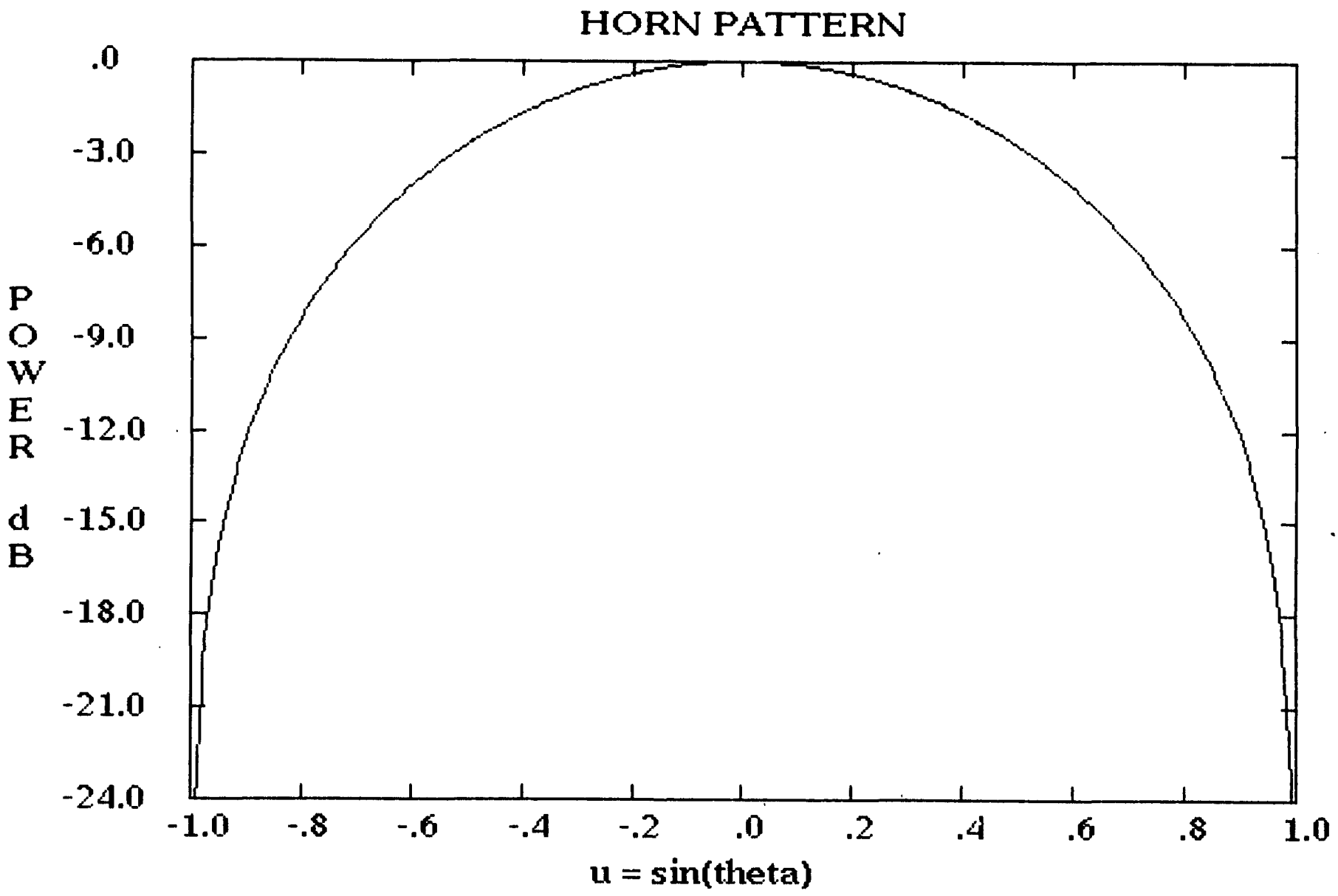

Fig. 29. Transmitter horn antenna H-plane pattern.

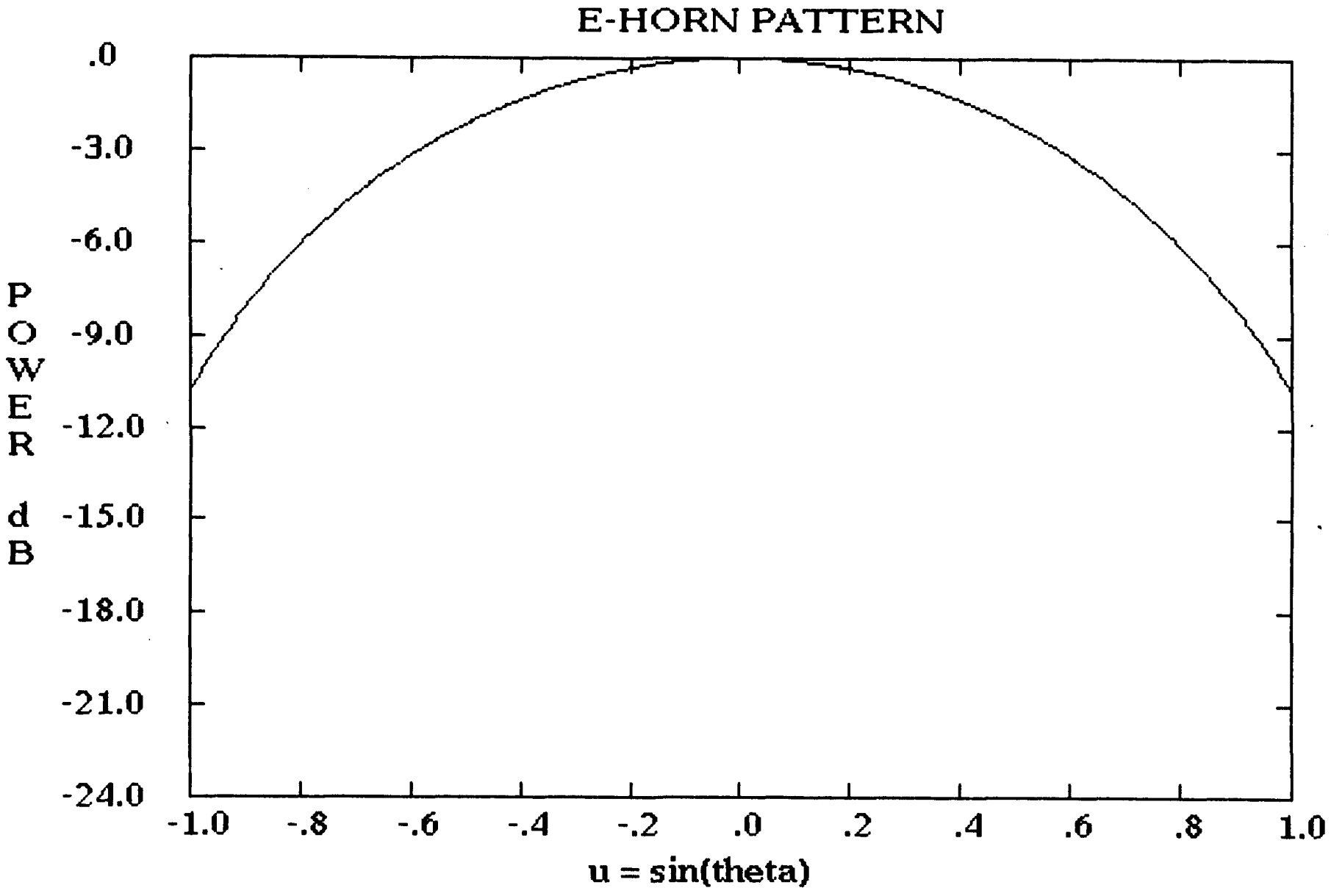

Fig. 30. Transmitter horn antenna E-plane pattern.

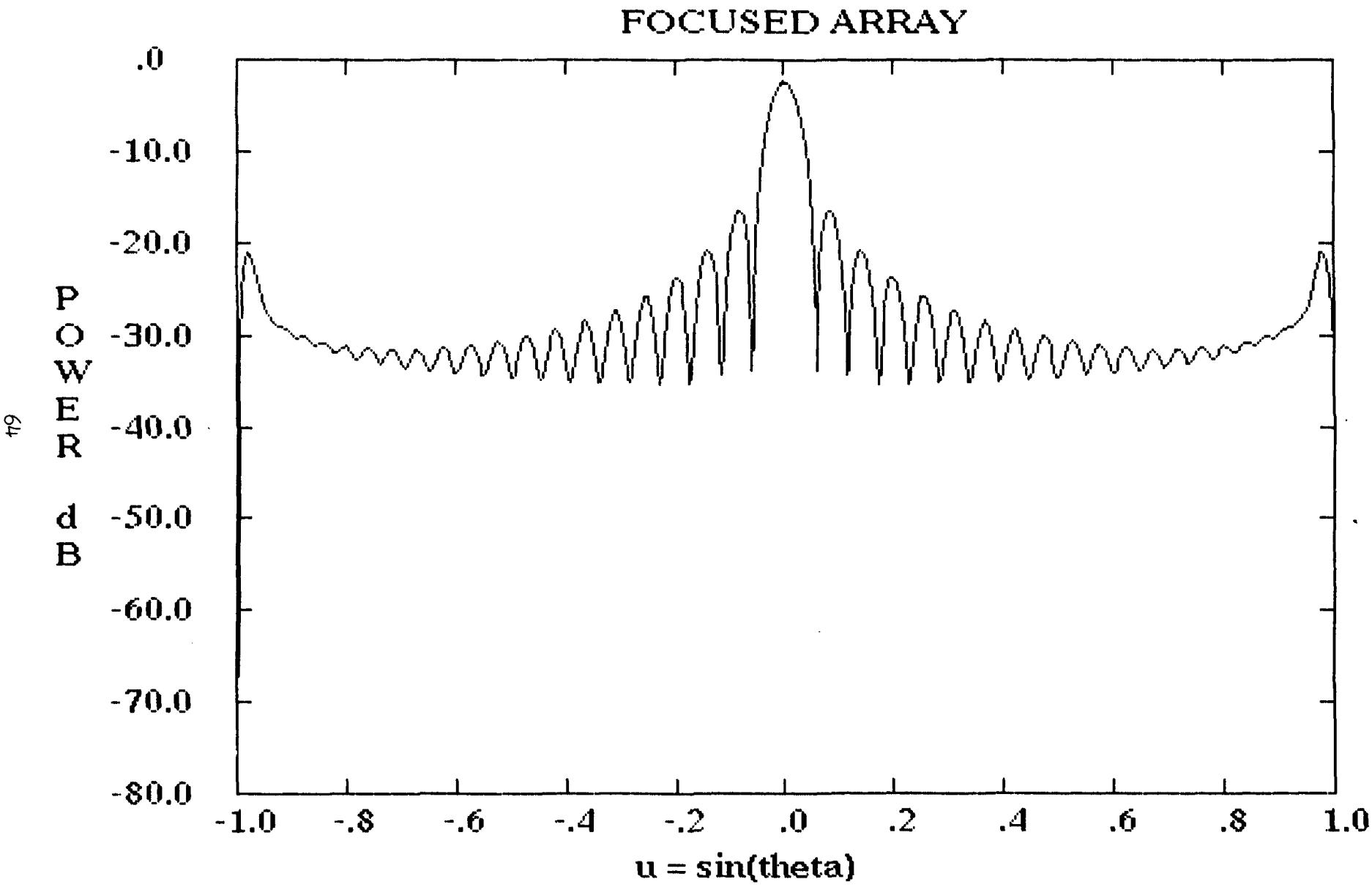

Fig. 31. H-plane focused array pattern, scan u=0.

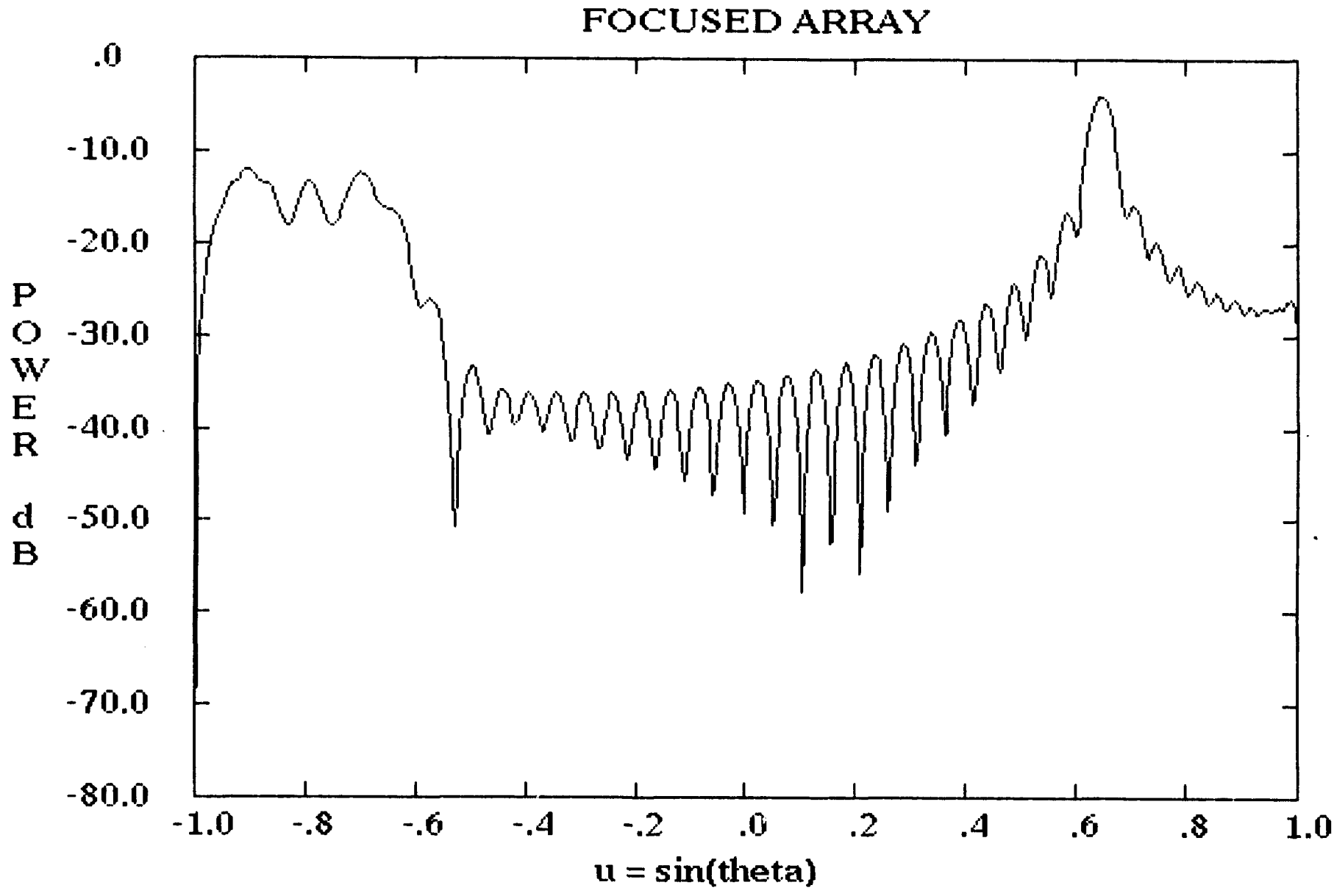

Fig. 32. H-plane focused array pattern, scan u=.64516.

plied to the phase comparator. This ensures that the received echoes will be coherent with the reference. The I and Q quadrature outputs of the phase comparator will be amplified and filtered by a pair of d-c coupled amplifiers. The resultant signals will each then be applied to a slow A/D converter. Several samples may be averaged if desired and the outputs from each element are input to the digital beamformer. This might use a 32 point hardware FFT chip using ECL logic that can produce 32 beam outputs each with a resolution of 5 cm in 0.3 microseconds. This gives 32 horizontal focused beams at one forward position of the array. A higher FFT size can be used if more image resolution is desired. A control computer is used for the A/D converters and FFT hardware through an interface. The transmitter and receiver configuration is illustrated in Fig. 34.

5.4 Data Acquisition and Digital Signal Processing

The data processing requirements have been greatly reduced by eliminating unnecessary computations. As the line array moves in a forward direction forming a new rectangular array for each forward position, scanning the entire field of view for each of these new positions would be time consuming and redundant. A simpler solution is to scan only the new area included in each forward position. The synthetic array imaging concept is illustrated in Fig. 33. Each horizontal array making up the rectangular synthetic array corrects for its own phase plus that of the transmitter position. The horizontal array then forms focused beams in the y direction. The array then moves ahead one location and the process is repeated. In this manner, beams in the y direction are formed about every 5 cm in the x direction. When all 32 horizontal arrays have been formed, they are summed in the y-direction forming a 32 x 32 element rectangular array, with 32 or more beams over the horizontal strip in the common field of view. When the array moves to the next forward position, only the new horizontal array forms its 32 beams over the new image area, and a new rectangular array is formed by adding this to the previous 31 horizontal array outputs. This is possible because of the separability of the x and y beamforming coordinates into the x and y arrays respectively.

The resulting number of computations required for each forward position

SYNTHETIC ARRAY IMAGING

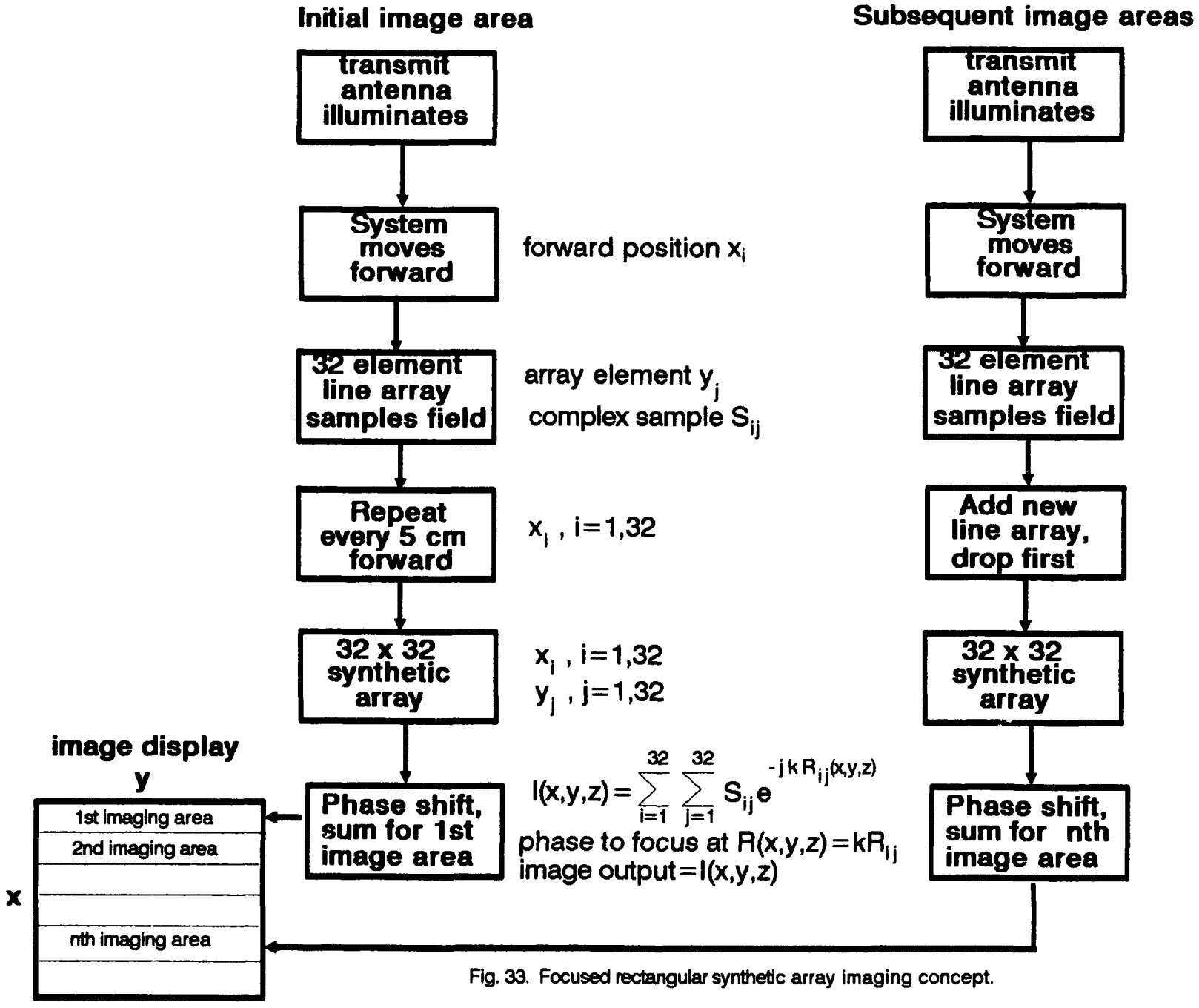

Fig. 33. Focused rectangular synthetic array imaging concept.

SYSTEM T/R MODULE

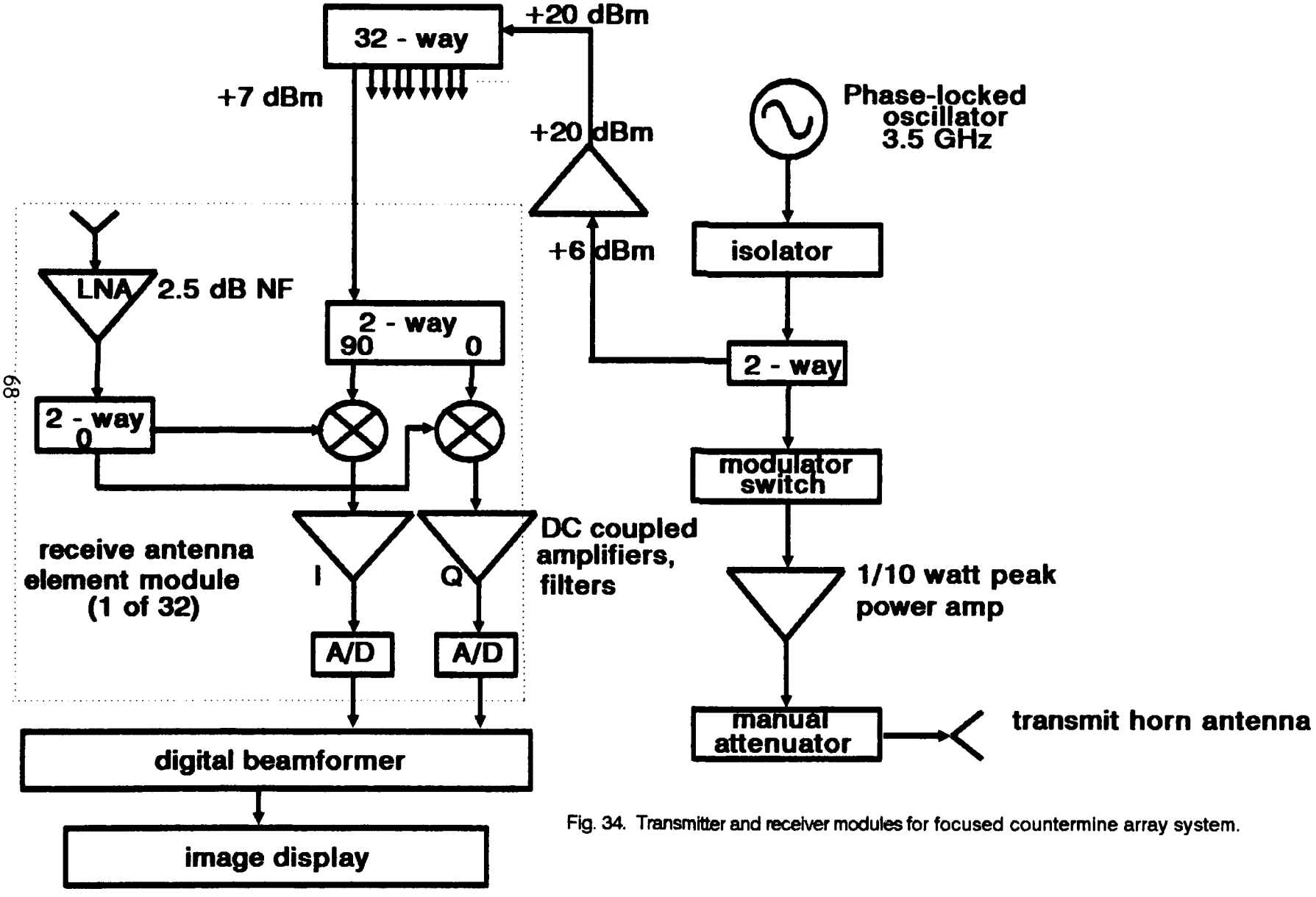

Fig. 34. Transmitter and receiver modules for focused countermine array system.

there are 32 horizontal beams x 32 elements or 1024 complex multiplications for each new array. The rectangular array output is then computed for each of the 32 beams in the new forward position by summing the horizontal array outputs which requires another 32 elements (longitudal) x 32 beams or a total of only 2048 complex multiplications to form the 32 beams with the 1024 element rectangular array in each 5 cm wide horizontal strip. At a speed of 10 km per hr this would require the computations to be completed to form the image in 16 msec. This is easy to accomplish for only 2048 complex multiplications so even higher rates of forward motion would be possible.

5.5 Detection and Imaging

The images in the sequential horizontal strips as the system moves in a forward direction would be displayed in real time in color or gray level on a display which is continuously monitored by an observer. Detection and identification would be based upon knowledge of the scattering and image characteristics of anti-tank mines with this system.

5.6 Mechanical Considerations

All of the system electronics including the transmitter would be contained inside of the countermine vehicle. The transmit antenna and receive array would be very light in weight, and could be mounted on an extension from the countermine vehicle supported by trusses of sufficient length to obtain the required standoff distance. The proposed forward scattering focused array is largely insensitive to absolute or relative vertical and horizontal motion of the transmit and receive arrays. The standoff given by such a structure combined with the greater than 1 m standoff of the system presents a feasible solution to this problem. Because of the light weight of the system, a structure could probably designed for use with existing vehicles.

5.7 Cost Factors

The major cost factors for the proposed system are enumerated below:

(1) 32 receiver modules
(2) data acquisition, processing and display hardware
(3) 32 element dipole receiver array
(4) mechanical support
(5) transmitter and electronics

An accurate estimate of the total cost requires a more detailed specification of the experimental conditions desired. However the proposed design is simple and could be designed and fabricated at low cost.

5.8 Feasibility of Approach

The two most important feasibility issues are the ability of the proposed concept to

1) significantly reduce ground surface reflections, thereby enhancing signal-to-clutter ratio using bistatic oblique forward scattering at the Brewster angle;

2) attain a high three-dimensional resolution using a microwave phased array focused in its near field.

The corollaries of these issues are the ability of the system to

1) detect subsurface plastic and metal mines with a high signal-to-clutter ratio.

2) identify and classify mines by shape and signature determination.

A third issue is the feasibility of the radar system design required to achieve the desired performance. Besides the required hardware and software design and fabrication, there are the questions of speed of forward motion and system cost.

The results of this project have conclusively demonstrated that surface reflections are significantly reduced, and subsurface target detection enhanced. The experimental results have shown that both metal and plastic

mines can be detected with a high signal-to-clutter ratio because of the reduction of surface reflections with the Brewster angle propagation geometry. High resolution three-dimensional images of the plastic and metal anti-tank mines have demonstrated that distinctive signature and shape information can be obtained from these images so that the mines are readily identifiable.

Feasibility of the system design depends upon the cost and complexity of the hardware and software, and whether it can be designed to adequately meet the system requirements. The system described above requires only simple, inexpensive hardware, and the data processing incorporates a number of simplifications which enhances signal processing speed, and allows a high rate of forward motion.

The Phase II experiment has been designed to test a system which closely resembles the final proposed countermine system. This experimental system will include the proposed transmitter and transmit horn antenna, the 32 element dipole antenna array, and one receiver module into which the 32 element outputs will be sequentially switched in order to save cost. The proposed operational system will use 32 individual receiver modules of the same design which will be used in parallel by the array. The Phase II experiment will also use similar signal processing software to that in the operational system.

The ability to test a system during the Phase II experiments that closely resembles the operational system will enable a conclusive verification of the feasibility of this system. This Phase II experimental simulation will be performed at a relatively low cost so that the risk is minimized.

6.0 PHASE II EXPERIMENTS

6.1 System Design

The experiments will use a 32-element array since this is the same as the proposed system. In order to reduce the required expense for the digital beamforming modules, only one module will be fabricated, and the 32 elements will be sequentially switched through this one module. This module will contain an RF amplifier, a pair of quadrature mixers, a low pass filter and a pair of A/D converters which sample the I and Q signal components.

6.2 System Components

The block diagram of the proposed Phase II system is presented in Fig. 35. It consists of four main sections: the 32-element array, the receiver, the control computer, and the transmitter. A variety of array configurations were considered in the development of this plan. The design chosen was both cost effective and reliable. It initially calls for one prototype receiver module to be constructed and connected to each of the S-band antennas sequentially through four eight-way switches. Each of the elements in turn is thus connected to the A/D converter subsystem and the analog outputs of the receiver are digitized and stored in memory. This will allow experimentation to procees while modifying the receiver design.

The design of the receiver is also of interest. The central component is a 3.5 GHz oscillator which is used as both the microwave source in the transmitter and the phase reference for the receiver. There is no special requirement on its stability since it serves as the source of both these signals. The quadrature phase comparator contains two identical S-band mixers. Since the waveforms applied to the RF and LO ports are identical in frequency, the output of each mixer will have two components: the sum (7 GHz) and the difference (baseband). The amplitude of this low frequency signal will be directly proportional to the phase difference between the inputs. This is the desired output of the mixers. A low pass filter will be used to separate it from the unwanted microwave component. (It is interesting to note that a significant constraint on the mixer is that the IF port must be dc coupled.) A quadrature power divider is used to provide a second reference channel with a 90 degree phase shift. In this manner, both I and Q signals are produced, and the phase can be measured without ambiguity.

Several possible designs were considered for implementation of the phase comparator. In the chosen method the mixers operate directly at microwave frequencies. A more conventional approach might have been to beat down the S-band signals to an IF and then apply them to the phase comparator. Since excellent mixers are available in the 3.5 GHz band it was decided to use this approach and save on additional complexity and unnecessary compo-

PHASE II EXPERIMENTAL SYSTEM

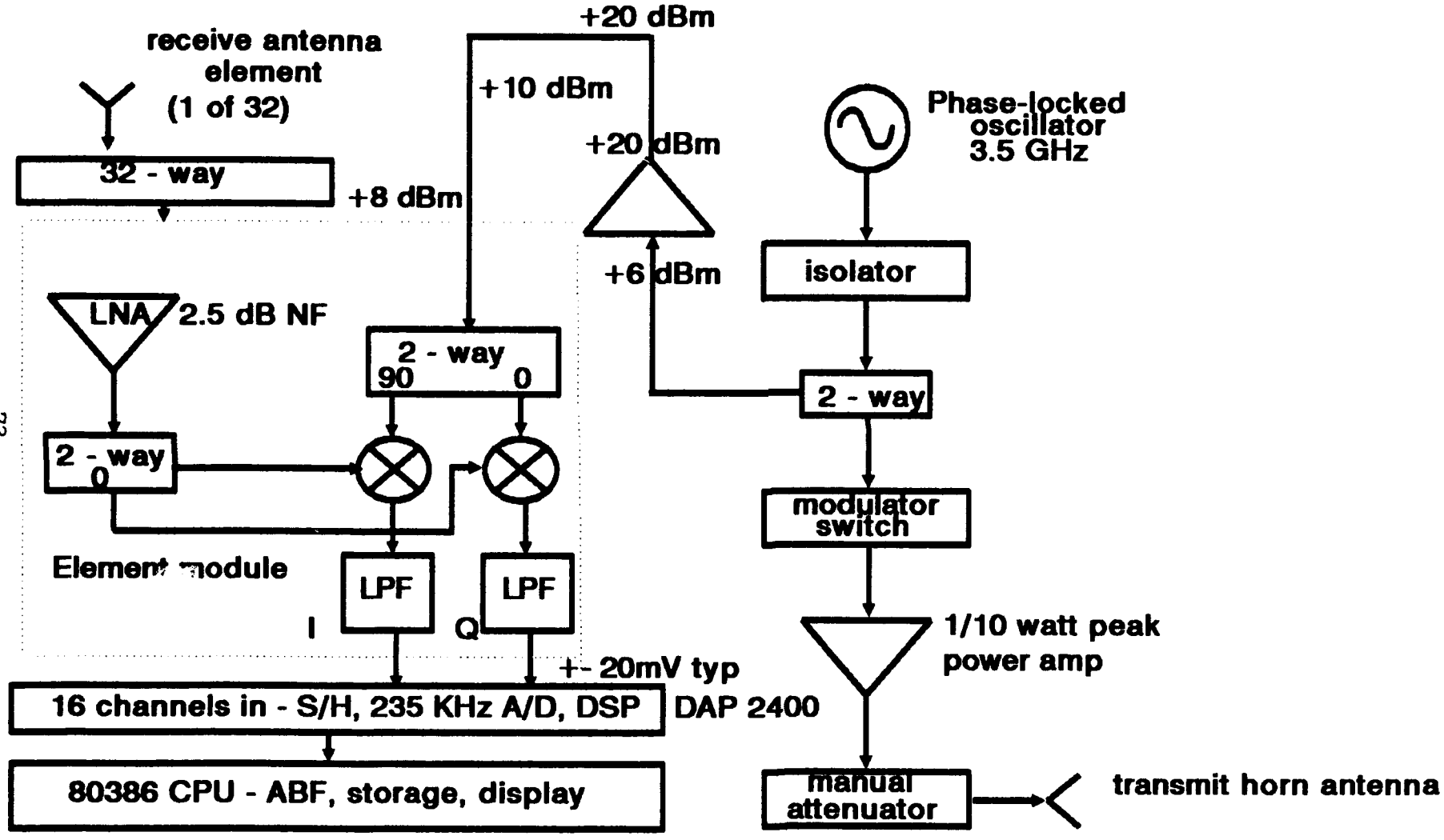

Fig. 35. Phase II experimental system diagram.

ing of the output signals and the digitizing process should not be difficult.

A variety of flexible, 12-bit A/D converters are available. With sampling speeds commonly in the range of 200 - 300 kHz it will be possible to choose from a large selection of commercial products. It is very desirable to use an integrated computer and sampling system if possible. This will not only lessen the complexity of interfacing several instruments but it will also reduce the time needed for processing since no data transfer procedure is required. Several companies produce A/D boards which may be installed directly in an expansion port of an 80386 computer. They are operated directly from appropriate control software in the computer. Many of these units contain multiple channels (typically 16) and some are available with built in sample/hold circuits for even greater flexibility.

The transmitter is a small sub-assembly which includes a 1/10 Watt power amplifier and a switch controlled by the central computer. The programming will specify the sequence where each transmitter is activated. The microwave reference will be supplied by 1/2" diameter foam-dielectric coaxial cable. The attenuation for a 20' length will be quite small (about 1 dB). The choice of power levels was based on experience with usable signals in previous short range indoor experiments. A 20 W TWT amplifier will be used if an additional 20 dB of transmitted power is required for adequate SNR. Previous tests have not required this additional power. The block diagram of this equipment is similar to that in the proposed system design.

In summary it should be noted that in large part this entire assembly may be purchased as commercially produced components. This improves the performance a great deal over parts built specifically for this project. It also increases the flexibility of the system since the components can often be applied to other experiments than those originally specified.

6.2.1 Antenna Array

The chosen frequency for the Phase II experiment is S-band at 3.5 GHz. With a wavelength of 8.57 cm., a 32-element array of dipoles spaced by 0.775 wavelengths will have a length of 2.1254 m.

The test array for Phase II will be a 32-element horizontal linear array

of vertically polarized dipole antennas backed by a ground plane. The dipoles will be placed $\lambda/4$ in front of the ground plane, and each will be center-fed by a balanced line as illustrated in Fig. 36. The balun feeds the dipole arms and the supporting legs in parallel. For a distance of $\lambda/4$ above the ground plane the input impedance of the supporting legs is very high and negligible current flows on them, so only the dipole is fed. Each dipole has an image in the ground plane, increasing the effective number of elements and directivity of the array.

This type of array has been chosen since design techniques including mutual coupling and active impedance calculations are well known. Since there are only eight elements, the active impedance will vary widely from element to element. Since the individual element outputs will be digitized, their active impedances must be individually matched to each receiver line in order to realize desired currents on each element. However, since the beamforming will be done digitally with full amplitude and phase control over the digital outputs before combining, there is considerable flexibility in the design and matching of the array elements.

6.2.2 Receiver

There will be one receiver module fabricated for the array elements which will provide the I and Q element signals to the digital beamformer by sequentially switching the elements to the module. Each consists of a low noise preamplifier with 2.5 dB noise figure after which the signal is split before input to the pair of quadrature mixers. The input signals are mixed with the 3.5 GHz source, providing baseband I and Q signals after the low pass filters remove the high frequency component. The element receiver assembly is shown in Fig. 35.

Each of the 32 pairs of I and Q outputs will then be input to a general purpose A/D and digital signal processing board which simply uses an expansion port of an 80386 computer. The board tentatively chosen for this task is the DAP 2400 board illustrated in Fig. 37. There are several major advantages to using this approach with this board. The channels are simultaneously sampled by the sample and hold and then input to the 235 KHz 12-bit A/D.

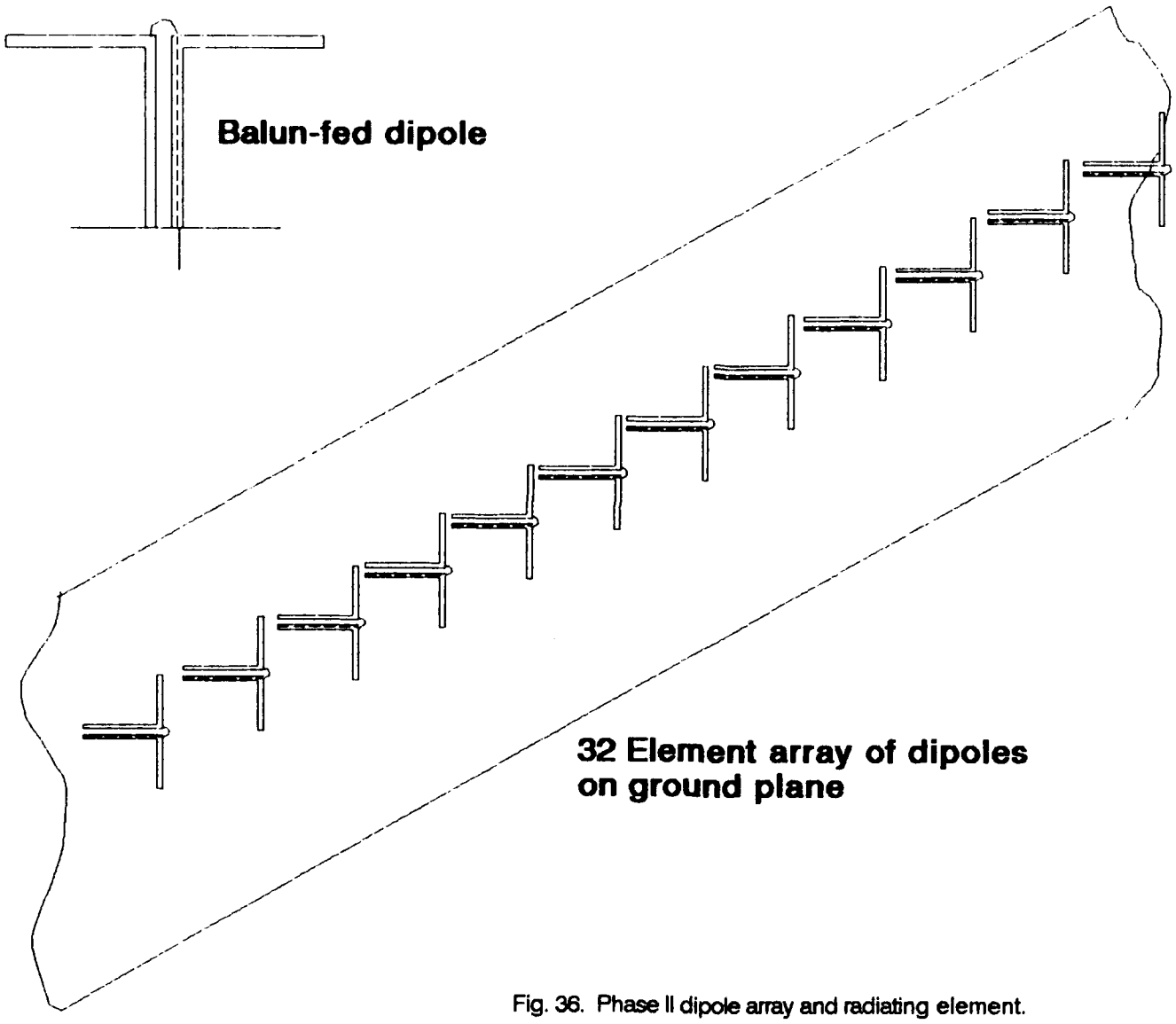

Fig. 36. Phase II dipole array and radiating element.

channel. The data aquisition processor has an on-board 80186 16 MHz CPU with 24K RAM for data acquisition control and digital signal processing. The data is then read by the 80386 computer where the digital adaptive beamforming is performed.

For measurement of the adapted pattern, at each measurement angle the data is sampled and the output of the array is computed using the adaptive weights. The array output is then stored and output to a high resolution display. The DAP board provides complete and flexible data acquisition control, digital signal processing, and adaptive beamforming from the console of an 80386 computer at relatively low cost ($7K including computer).

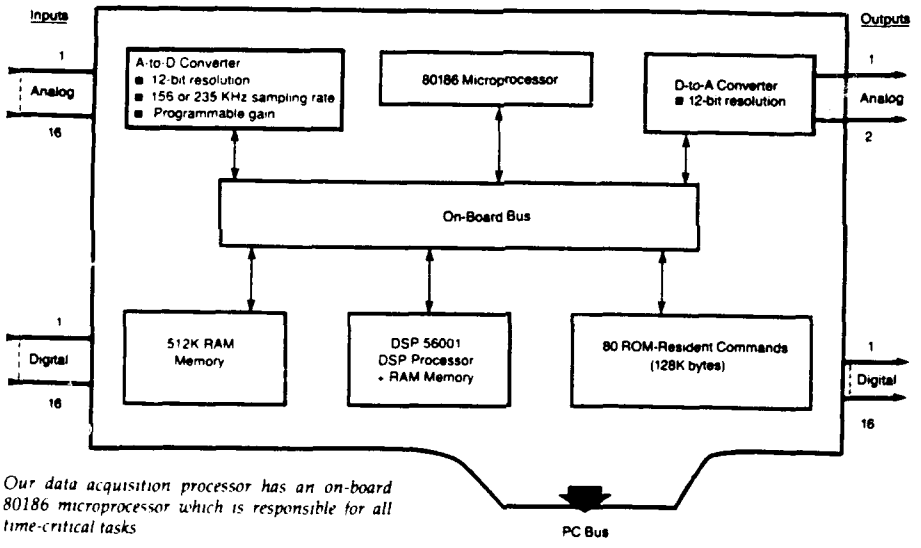

Fig. 37. Data Acquisition Processor for Phase II experiments.

6.2.3 Transmitter

The transmitter source is shown in Fig. 35. The RF source is the 3.5 GHz phase locked oscillator which provides an amplified CW signal for the transmit horn antenna, as well as a reference for each of the receive elements

in the array. The probe antenna will be horn antenna fed from WR284 waveguide and flared in the E-plane.

6.3 Experimental Plan

The experimental setup will allow real synthetic aperture measurements to be taken by forward motion of the entire system. The experiments will test most of the aspects of the proposed system design to allow a refinement of the design.

The tests will be done with various buried mine targets and other buried objects of interest. The experiments will be done in both dry and moist soil, and the dielectric constant and conductivity will be determined for the refraction correction in the beamforming software.

The experiments will form a 1024 element rectangular focused synthetic array by moving the 32 element line array sequentially to 32 forward positions. At each position the data will be sampled and processed as described previously. The images formed will be studied to determine signal-to-clutter ratio and signature characteristics.

7.0 REFERENCES

[1] W. J. Graham, "A New Fresnel Region Approximation," IEEE International Symposium on Antennas and Propagation, Digest, Vancouver, BC, June 1985.

[2] J. A. Stratton, Electromagnetic Theory, McGraw-Hill, New York, 1941.

[3] A. Erdelyi, "Asymptotic Representations of Fourier Integrals and the Method of Stationary Phase," J. Soc. Ind. Appl. Math., col. 3, pp. 17-27, 1955.

[4] T. T. Taylor, "Design of Line Source Antennas for Narrow Beamwidth and Low Side Lobes," IRE Trans. Antennas Propagat., vol. AP-7, pp. 16-28, Jan. 1955.

[5] W. J. Graham, "Analysis and Synthesis of Axial Field Patterns of Focused Apertures," IEEE Trans. Antennas Propagat., vol. AP-31, pp. 665-668, July 1983.

[6] _____, "The Fresnel Transform Approximation for Aperture Field Patterns in the Fresnel Region," submitted to IEEE Trans. Antennas Propagat.

[7] _____, "Fresnel Region Imaging with a Linear Array," International conference on Acoustics, Speech and Signal Processing, Proceedings, Tokyo, Japan, April 8-11, 1986.

[8] _____, "Focused Countermine Array for Microwave Detection and Destruction of Mines," Final Report, Contract No. DAAH01-89-C-0797, Graham Research Report No. TR-89-001-02, February, 1990.